https://doi.org/10.5194/wes-2026-90
Preprint. Discussion started: 17 June 2026

eawe european academy of wind energy
Open Access WIND ENERGY SCIENCE DISCUSSIONS

An Open-Access Integrated Hierarchical Optimization Framework applied to a 15 MW Medium-Speed Offshore Wind Turbine Drivetrain

Felix Christian Mehlan[1] and Amir R. Nejad[1]

[1]Norwegian University of Science and Technology (NTNU), Professor JHL Vogts veg 1a, 7050 Trondheim, Norway

Correspondence: Felix Christian Mehlan (felix.c.mehlan@ntnu.no)

Abstract. This work presents an open-access hierarchical, physics-based optimization framework for medium-speed wind turbine drivetrains. The methodology combines mixed-integer architecture exploration with continuous gradient-based refinement, enabling simultaneous optimization of gearbox topology, stage-ratio distribution, gear geometry, shaft sizing, and bearing selection under ISO 6336, ISO 281, and DIN 743 constraints.

Compared to previous design frameworks based on empirical scaling laws, such as WISDEM, the integrated stage-ratio optimization achieved drivetrain mass reductions of approximately 4–5% while satisfying all design constraints.

Convergence studies demonstrated that the proposed hierarchical optimization strategy efficiently handles the complex mixed-integer design landscape, producing competitive gearbox solutions in <2.5 h on a desktop computer.

Applied to a 15 MW offshore wind turbine, the optimized medium-speed drivetrain achieved a total mass of 274.2 t, corresponding to a 31.5% reduction relative to the direct-drive reference while maintaining comparable efficiency (97.2%). The results demonstrate that integrated hierarchical optimization enables competitive drivetrain solutions for next-generation offshore wind turbines.

1 Introduction

The rapid upscaling of offshore wind turbines toward the 15–20 MW class has significantly increased the demands placed on drivetrain systems. Larger rotor diameters and higher aerodynamic loads require drivetrains capable of transmitting extremely high torque while maintaining low nacelle mass, high efficiency, and long-term reliability under harsh offshore operating conditions. In floating offshore wind applications, drivetrain mass becomes even more critical, as nacelle weight directly affects tower-top loads, platform dynamics, and mooring system response (Barter et al., 2023).

Traditionally, offshore wind turbine drivetrains have followed two principal design philosophies: direct-drive systems and geared medium-speed systems. Direct-drive concepts eliminate the gearbox and thereby reduce mechanical complexity, but require very large low-speed generators that substantially increase nacelle mass and material usage. Medium-speed drivetrains, in contrast, combine gearboxes with lighter and more compact generators (Nejad and et al., 2022). However, the design of geared drivetrains introduces a highly coupled optimization problem that involves gearbox topology and component design decisions.

https://doi.org/10.5194/wes-2026-90
Preprint. Discussion started: 17 June 2026

eawe european academy of wind energy
Open Access WIND ENERGY SCIENCE DISCUSSIONS

Existing drivetrain design tools only partially address this complexity. System-level frameworks such as WISDEM's DrivetrainSE (National Renewable Energy Laboratory (NREL), 2024) are based on empirical scaling models that are suitable for conceptual trade-off studies but insufficient for detailed mechanical synthesis. In contrast, commercial software such as KISSsoft (KISSsoft AG, 2022a), Romax Spectrum (Romax Technology Ltd., 2024), and FVA-Workbench (Forschungsvereinigung Antriebstechnik e.V. (FVA), 2024) provide standards-based gear and bearing analysis according to ISO 6336, ISO 281, and DIN 743, but generally assume predefined drivetrain architectures and therefore offer limited capability for simultaneous architecture and component optimization. Consequently, a methodological gap remains between system-level drivetrain synthesis and detailed component-level design.

Previous academic studies have investigated gearbox design optimization. However, most approaches either optimize predefined gearbox layouts or separate architecture synthesis from detailed component design (see Section 2 for a detailed review).

To address this limitation, this paper presents an open-access hierarchical optimization framework for medium-speed offshore wind turbine drivetrains. The proposed methodology combines mixed-integer architecture exploration with continuous gradient-based optimization to simultaneously optimize gearbox topology, transmission ratio allocation, gear geometry, shaft dimensions, and bearing sizing. The framework employs physics-based analytical models and enforces standards-based constraints according to ISO 6336, ISO 281, and DIN 743. Furthermore, all objective and constraint functions are formulated in a fully differentiable manner, enabling the use of automatic differentiation and efficient gradient-based optimization techniques.

The framework is applied to the design of a 15 MW floating offshore wind turbine drivetrain based on the MADE4WIND reference configuration (Rezaei et al., 2024). The optimized medium-speed drivetrain is benchmarked against the IEA 15 MW direct-drive reference turbine to evaluate trade-offs between mass, efficiency, and reliability (Gaertner et al., 2020). Results demonstrate that the proposed framework enables substantial drivetrain mass reductions while maintaining comparable efficiency, highlighting the importance of integrated drivetrain synthesis for next-generation offshore wind turbines.

The remainder of this paper is organized as follows. Section 2 reviews related optimization research. Section 3 presents the proposed hierarchical optimization framework. Section 4 discusses validation and optimization results. Finally, Section 5 summarizes the key findings and outlines directions for future work.

2 Background

Gearbox optimization research generally falls into three categories: (i) architecture and configuration synthesis, (ii) detailed component-level optimization for strength, efficiency, and NVH, and (iii) reliability-based or robust optimization under uncertainty.

Early multi-stage gearbox design studies integrated dimensional and configuration design using a metaheuristic search to minimize gearbox volume under spatial constraints (Chong et al., 2002). More recently, concept-level analytical toolboxes have been proposed to link configuration synthesis with preliminary mechanical sizing. For example, Zeller et al. (2024) present a gearbox–generator design framework that determines suitable multi-stage topologies and ratio distributions based on drive-cycle data and generator efficiency maps. An ideal overall transmission ratio is first identified, after which feasible partial ratios and gearbox concepts are enumerated and evaluated using analytical strength calculations and weighted scoring.

https://doi.org/10.5194/wes-2026-90
Preprint. Discussion started: 17 June 2026

Several studies have explicitly addressed the allocation of transmission ratios in multi-stage gearboxes. Huynh and Nguyen (2025) formulate ratio distribution in a three-stage spur-helical gearbox as a constrained optimization problem, combining analytical sizing relations with differential evolution to minimize volume while enforcing uniform contact-fatigue strength and oil-bath lubrication constraints.

For planetary gear trains, Stefanović-Marinović et al. (2025) propose a discrete multicriteria optimization framework for a three-stage planetary gearbox, considering volume, mass, efficiency, and production cost. Pareto-optimal solutions are generated by enumerating admissible gear parameter combinations and selecting preferred configurations using weighted scalarization.

A substantial body of work focuses instead on macro- and micro-geometry optimization to reduce excitation sources such as static transmission error (STE) and mesh stiffness fluctuations (Garambois et al., 2017). Robustness to manufacturing errors has been examined using Monte Carlo simulation and Taguchi-based statistical tolerancing (Driot and Perret-Liaudet, 2006). These studies provide high-fidelity NVH modeling but operate on predefined gearbox topologies.

Other research formulates multi-objective optimization problems to minimize volume and power loss while incorporating mechanical and tribological constraints such as pitting, scuffing and wear (Patil et al., 2019). Reliability-based design optimization (RBDO) frameworks extend this by introducing probabilistic reliability indices into gearbox synthesis (Karmi et al., 2024). However, these methods typically assume fixed drivetrain architectures and do not explicitly couple transmission ratio allocation with ISO-based gear strength, shaft sizing, and rolling bearing lifetime within a unified hierarchical optimization structure.

Collectively, prior work either optimizes predefined drivetrain configurations using detailed component models, explores ratio allocation under simplified strength assumptions, or performs architecture synthesis using partially coupled mechanics. Few approaches simultaneously address drivetrain topology, continuous stage-ratio allocation, gear macro-geometry, shaft sizing, and bearing selection within a unified, physics-based optimization framework that enforces ISO 6336 and ISO 281 constraints under realistic load spectra.

The methodology proposed in this work directly addresses this gap by embedding stage ratio allocation within a hierarchical drivetrain-level optimization procedure, in which architecture decisions, discrete gear geometry, shaft design, and rolling bearing lifetime are consistently coupled under standards-based mechanical constraints.

3 Methodology

3.1 Problem formulation

The gearbox design is formulated as a constrained, scalarized, multi-objective optimization problem that balances drivetrain mass and efficiency while satisfying kinematic, structural, and reliability requirements under representative operating loads.

https://doi.org/10.5194/wes-2026-90
Preprint. Discussion started: 17 June 2026

eawe european academy of wind energy
Open Access WIND ENERGY SCIENCE DISCUSSIONS

Table 1. Design variables for each planetary gear stage $k = 1...N_{\mathrm{St}}$. Variable limits LB and UB are based on KISSsoft AG (2022b).

Design variables		**Symbol**	**Format**	**LB**	**UB**
System level	Normalized gear stage ratio [-]	$(i_{\mathrm{St}}/i_{\mathrm{GB}})_k^{1/3}$	Continuous	0.75	1.5
Stage level (Discrete)	Number of planets [-]	$N_{\mathrm{P},k}$	Discrete	3	5
	Normal module [mm]	$m_{\mathrm{n},k}$	Discrete	8	50
	Tooth number of sun gear [-]	$z_{1,k}$	Discrete	17	50
	Tooth number of planet gear [-]	$z_{2,k}$	Discrete	17	100
	Tooth number of ring gear [-]	$z_{3,k}$	Discrete	17	150
Stage level (Continuous)	Profile shift coefficient of sun gear [-]	$x_{1,k}$	Continuous	-0.6	1.0
	Profile shift coefficient of planet gear [-]	$x_{2,k}$	Continuous	-0.6	1.0
	Overlap ratio [-]	$\epsilon_{\delta,k}$	Continuous	1.2	2.0
	Normalized face width [-]	$(b/m_{\mathrm{n}})_k$	Continuous	12	20
	Normalized sun shaft diameter [-]	$(d_{\mathrm{SS}}/d_{i,1})_k$	Continuous	0.1	1.0
	Normalized planet shaft diameter [-]	$(d_{\mathrm{PS}}/d_{i,\mathrm{PB}})_k$	Continuous	0.1	1.0

The overall optimization problem is stated as

$$\begin{aligned} \min_{\mathbf{x}} \quad & J(\mathbf{x}) \\ \text{s.t.} \quad & \mathbf{g}(\mathbf{x}) \leq \mathbf{0}, \\ & \mathbf{h}(\mathbf{x}) = \mathbf{0}, \\ & \mathbf{x}_{\mathrm{lb}} \leq \mathbf{x} \leq \mathbf{x}_{\mathrm{ub}}, \end{aligned} \tag{1}$$

where $\mathbf{g}(\mathbf{x})$ and $\mathbf{h}(\mathbf{x})$ represent the sets of inequality and equality constraints, respectively, and $\mathbf{x}_{\mathrm{lb}}$ and $\mathbf{x}_{\mathrm{ub}}$ denote the lower and upper bounds on the design variables.

3.1.1 Design objectives

The optimization objective is expressed as a weighted sum of normalized drivetrain mass and efficiency,

$$J(\mathbf{x}) = w \cdot \frac{W_{\mathrm{DT}}(\mathbf{x})}{W_{\mathrm{ref}}} + (1-w) \cdot \frac{\eta_{\mathrm{ref}} - \eta_{\mathrm{DT}}(\mathbf{x})}{\eta_{\mathrm{ref}}}, \tag{2}$$

where $\mathbf{x}$ denotes the vector of design variables, W_{DT} is the total drivetrain mass, η_{DT} is the drivetrain efficiency, and W_{ref} and η_{ref} are normalization references obtained from the lightest and most efficient designs in the Pareto set. The weighting parameter $w \in [0,1]$ controls the trade-off between pure mass minimization ($w = 1$) and pure efficiency maximization ($w = 0$).

https://doi.org/10.5194/wes-2026-90
Preprint. Discussion started: 17 June 2026

eawe european academy of wind energy
Open Access WIND ENERGY SCIENCE DISCUSSIONS

Table 2. Parameters for the MADE4WIND 15 MW drivetrain case study.

Parameter	Symbol	Value
Rated power	P_0	15 MW
Rated rotor speed	n_0	7.56 rpm
Pressure angle	α_n	20 deg
Addendum coefficient	h_a	1.0
Dedendum coefficient	h_f	1.25
Rim thickness coefficient sun	$s_{\mathrm{R},1}$	1.2
Rim thickness coefficient planet	$s_{\mathrm{R},2}$	1.2
Rim thickness coefficient ring	$s_{\mathrm{R},3}$	3.5
Root radius factor	ρ_fPf	0.38
Required root safety	$S_{\mathrm{F,min}}$	1.56
Required flank safety	$S_{\mathrm{H,min}}$	1.25
Required bearing nominal lifetime	$L_{\mathrm{10h,min}}$	25 years
Permissible gear stage ratio deviation	Δi_st	2%
Permissible bending stress	σ_Flim	430 N/mm^2
Permissible contact stress	σ_Hlim	1500 N/mm^2
Young modulus	E	206 MPa
Poisson's ratio	ν	0.3
Density	ρ	7850 kg/m^3
Mean roughness	R_z	4.8 μm

Table 3. Constraints

Constraint		Equation	Reference
Gears	Flank safety	$g_1(\mathbf{X}) = S_{\mathrm{H,min}} - S_\mathrm{H} < 0$	ISO (2006)
	Root safety	$g_2(\mathbf{X}) = S_{\mathrm{F,min}} - S_\mathrm{F} < 0$	ISO (2006)
	Adjacency condition	$g_6(\mathbf{X}) = d_{\mathrm{a},2} - 2a\sin(\pi/N_\mathrm{p}) < 0$	Qin et al. (2018)
	Assembly condition	$h_1(\mathbf{X}) = \mod(z_3 + z_1, N_\mathrm{p}) = 0$	Qin et al. (2018)
	Transmission ratio condition	$g_5(\mathbf{X}) = \frac{\hat{i}_\mathrm{st} - i_\mathrm{st}}{i_\mathrm{st}} - \Delta i_\mathrm{st} < 0$	Qin et al. (2018)
Planet bearings	FLS safety	$g_3(\mathbf{X}) = L_{\mathrm{10h,min}} - L_\mathrm{10h} < 0$	ISO (2007)
Planet & sun shafts	ULS safety	$g_4(\mathbf{X}) = S_{\mathrm{ULS,min}} - S_\mathrm{ULS} < 0$	DIN (2012)

3.1.2 Design variables

The design variables are organized hierarchically into system-level, stage-level discrete and stage-level continuous parameters, as summarized in Table 1.

https://doi.org/10.5194/wes-2026-90
Preprint. Discussion started: 17 June 2026

eawe european academy of wind energy
Open Access WIND ENERGY SCIENCE DISCUSSIONS

At the system level, the normalized gear stage ratio $(i_{\mathrm{St}}/i_{\mathrm{GB}})_k^{1/N_{St}}$ defines the distribution of the total gearbox ratio among the individual stages. Discrete stage-level variables define the planetary gear topology and include the number of planets, the normal module, and the tooth numbers of the sun, planet, and ring gears.

Continuous stage-level variables refine the geometry for a given topology and comprise the profile shift coefficients, overlap ratio, normalized face width, and normalized sun and planet shaft diameters.

3.1.3 Design constraints

Design feasibility is enforced through physics-based constraints expressed as inequality or equality conditions on the design variables, as summarized in Table 3. Gear-related constraints include minimum flank and root safety factors according to ISO 6336, geometric adjacency and assembly conditions for planetary stages, and a transmission ratio consistency constraint. Bearing reliability is enforced through a fatigue limit state constraint based on nominal bearing life in accordance with ISO 281, while shaft integrity is ensured through an ultimate limit state safety constraint applied to the sun and planet shafts according to DIN 743.

3.2 Physics-based component models

The optimization framework employs physics-based component models to evaluate gearbox geometry, internal loads, mass, efficiency, and reliability. These models provide the quantitative inputs required for the objective function and constraint evaluation.

Gear geometry (A3) is defined using standardized normal modules and discrete tooth numbers, while continuous profile shift coefficients, facewidth parameters, and overlap ratios are used to refine the macro- and micro-geometry. From the resulting geometry, working pressure angles, center distances, and contact ratios are derived.

Internal loads (A3) are computed from the applied drivetrain torque and operating speeds using analytical load transfer path models. Load calculations assume equal load sharing among the planet gears and neglect internal dynamic effects. The tangential, radial and axial forces acting on gears, bearings, and shafts are evaluated. Both fatigue limit state (FLS) and ultimate limit state (ULS) load cases are considered. Fatigue loading is represented through equivalent stress cycles obtained from stress cycle counting of time-domain load histories, while extreme loading conditions are used for ULS checks. Representative drivetrain loads, including torque and speed histories, are provided as inputs from aeroelastic simulations performed with OpenFAST.

Gear strength and bearing reliability (A5) are evaluated using established design standards. Gear root and flank safety factors are computed according to ISO 6336. Bearing reliability is assessed using the nominal bearing life formulation based on ISO 281, with bearing capacities and dimensions taken from manufacturer catalog data. Shaft strength is verified against ultimate limit state requirements according to DIN 743.

Drivetrain efficiency (A4) is evaluated using an analytical gear mesh loss model based on the Niemann formulation (Niemann and Winter, 1983). Mesh losses are calculated as a function of contact forces, sliding velocities, and friction

https://doi.org/10.5194/wes-2026-90
Preprint. Discussion started: 17 June 2026

eawe european academy of wind energy
Open Access WIND ENERGY SCIENCE DISCUSSIONS

coefficients under elastohydrodynamic lubrication conditions and are aggregated to obtain stage-level and overall drivetrain efficiency.

Mass modeling (A4) combines analytical, catalog-based and empirical approaches. Gear and shaft masses are calculated using analytical volumetric formulations. Bearing masses are obtained from catalog data corresponding to the selected bearing sizes. The masses of the planet carrier and gearbox housing, which are not designed in detail in this work, are estimated using empirical relationships based on gearbox size.

3.3 Hierarchical optimization strategy

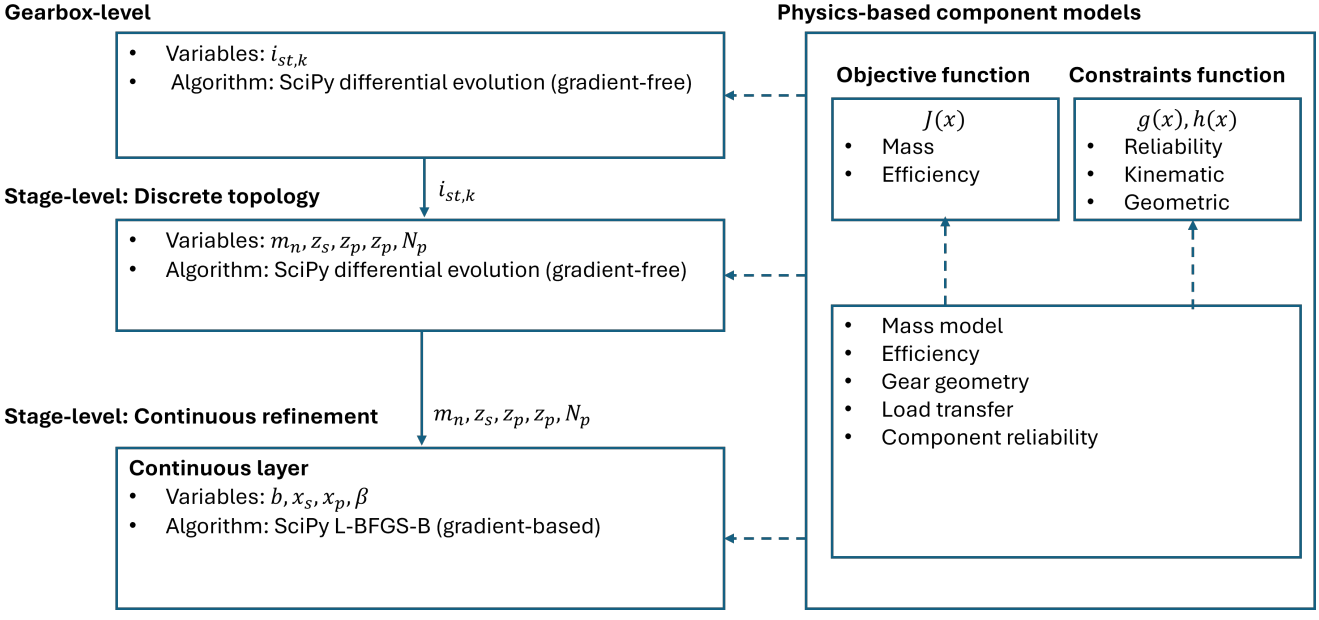

Figure 1. Gearbox design procedure.

The optimization framework adopts a three-layer hierarchical decomposition to efficiently address the large, mixed-integer and non-linear design space of multi-stage gearboxes. The hierarchy separates system-level architectural decisions, stage-level discrete topology selection, and continuous geometric refinement, enabling robust and computationally efficient optimization.

Layer 1: Gearbox-level optimization (stage ratios)

The outer layer determines the distribution of the total gearbox transmission ratio i_{gb} across the N_{st} individual stages. The design variables are the stage ratios $i_{\mathrm{st},k}$, which are constrained to satisfy

$$i_{\mathrm{gb}} = \prod_{k=1}^{N_{\mathrm{st}}} i_{\mathrm{st},k}.$$

To enforce this constraint, $N_{\mathrm{st}} - 1$ stage ratios are treated as independent variables, while the remaining ratio is derived. The optimization is performed using a global Differential Evolution (DE) algorithm, with the search conducted in logarithmic space

https://doi.org/10.5194/wes-2026-90
Preprint. Discussion started: 17 June 2026

eawe european academy of wind energy
Open Access WIND ENERGY SCIENCE DISCUSSIONS

$s_k = \ln(i_{\mathrm{st},k})$ to improve numerical conditioning and exploration. For each candidate ratio distribution, the objective function is evaluated by executing the stage-level optimizations for all stages, which are performed in parallel to reduce computational cost.

Layer 2: Stage-level optimization (discrete topology)

For a fixed stage ratio $i_{\mathrm{st},k}$, the intermediate layer searches for the optimal discrete gear topology defined by the integer design vector $\mathbf{x}_{I,k}$, comprising the sun, planet, and ring gear tooth numbers (z_s, z_p, z_r), the number of planets N_p, and the normal module m_n. Candidate topologies are first pre-screened to satisfy basic geometric and kinematic feasibility and to approximately match the target stage ratio. The discrete search is conducted using a Differential Evolution algorithm over the index of the pre-screened candidates. To improve efficiency, the normal module is explored in descending order, and the search is terminated early if no feasible continuous solution can be found for a given module size.

Layer 3: Stage-level optimization (continuous refinement)

The inner-most layer performs continuous optimization of the geometric design variables $\mathbf{x}_{C,k}$ for a fixed discrete topology. These variables include the profile shift coefficients of the sun and planet gears, the gear face width, and the overlap ratio. To enhance robustness, multiple feasible initial points are generated using quasi-random Sobol sampling. Starting from these points, a constrained local optimization is performed using a Sequential Least Squares Programming (SLSQP) solver, which minimizes the weighted objective function subject to the full set of non-linear constraints.

3.4 Differentiable implementation and gradient robustness

The inner continuous optimization layer relies on gradient-based solvers to efficiently handle the large number of non-linear constraints arising from ISO 6336, ISO 281, and DIN 743 formulations. However, standard analytical implementations of gear design equations contain numerous non-differentiable elements, including step functions, conditional branching, clipping operations, and implicit Newton iterations.

To enable robust gradient-based optimization, all objective and constraint functions were reformulated to be fully differentiable. This required several modifications:

- **Smoothing of conditional branches:** Piecewise ISO expressions and `if-else` conditions were replaced by smooth transition functions using hyperbolic tangent blending.
- **Removal of discontinuous operations:** Absolute values, clipping, and thresholding were replaced with smooth approximations (e.g. soft clipping).
- **Numerical safeguarding:** Potential singularities such as division by zero, square roots of small negative values, or inverse trigonometric domain violations were prevented using smooth safe guards.
- **Deterministic unrolling of Newton iterations:** Implicit root-finding procedures (e.g., for tooth form factors Y_F) were rewritten as a fixed number of explicitly unrolled Newton steps.

https://doi.org/10.5194/wes-2026-90
Preprint. Discussion started: 17 June 2026

eawe european academy of wind energy
Open Access WIND ENERGY SCIENCE DISCUSSIONS

– **Bearing catalog curve fits:** Discrete bearing catalog look-ups used to determine specifications such as dynamic load capacity were replaced by second-degree polynomial curve fits as functions of bearing geometry (outer diameter and width).

After enforcing full differentiability, analytical gradients were obtained using the `JAX` automatic differentiation framework. Compared to finite-difference approximations, analytical gradients significantly improve numerical robustness, reduce computational cost, and eliminate sensitivity to step-size selection. This is particularly important in the present problem, where constraint functions involve deeply nested non-linear expressions and repeated evaluations within the hierarchical optimization loops.

The resulting formulation enables stable and efficient Sequential Least Squares Programming (SLSQP) optimization in the continuous layer, which proved essential for reliable convergence.

3.5 Case study: 15 MW floating wind turbine drivetrain

The proposed hierarchical optimization framework is evaluated through a case study of a 15 MW medium-speed drivetrain intended for a floating offshore wind turbine. The study is based on the MADE4WIND project reference configuration for a turbine deployed on a tension-leg platform (TLP) at the Utsira Nord site (Rezaei et al., 2024).

Reference turbine and operating conditions

The reference turbine is derived from the IEA 15 MW offshore wind turbine, adapted for floating operation. Environmental conditions and design load cases (DLCs) follow IEC 61400-3-2 and include both fatigue and extreme loading scenarios. Global aeroelastic simulations are performed using OpenFAST to generate time-series rotor loads, including torque, thrust, shear forces, and bending moments. These loads are used as boundary conditions for drivetrain design and optimization, consistent with established decoupled load analysis practices.

Fatigue limit state (FLS) loads are derived from normal operation (DLC 1.2) using load duration distributions and stress cycle counting, while ultimate limit state (ULS) loads are obtained from the maximum responses across extreme DLCs (DLC 1.3–6.3), including emergency stop and extreme wind events (Tab. 4).

Drivetrain configuration and design space

As shown in Figure 2, a medium-speed drivetrain concept is investigated, comprising the main bearings, a multi-stage planetary gearbox, and a permanent-magnet synchronous generator. A medium-size gearbox with an overall transmission ratio of 1:50 is selected and coupled to a medium-speed generator to balance reliability and nacelle mass.

The main shaft is arranged in a four-point suspension, where two main bearings carry non-torque rotor loads and protect the gearbox from bending and axial forces. The gearbox may include two to four planetary stages, with the total transmission ratio fixed at the system level. Stage ratios, gear topology, and geometric parameters are optimized within the bounds defined in Section 3.

The scope of optimization is limited to the gearbox. Related work within the MADE4WIND project on integrated main-bearing and main-shaft assembly optimization will be presented by Gupta and Nejad Gupta and Nejad (2026). The generator and converter are outside the scope of this study and were designed separately within the project by INDAR and Ingeteam.

https://doi.org/10.5194/wes-2026-90
Preprint. Discussion started: 17 June 2026

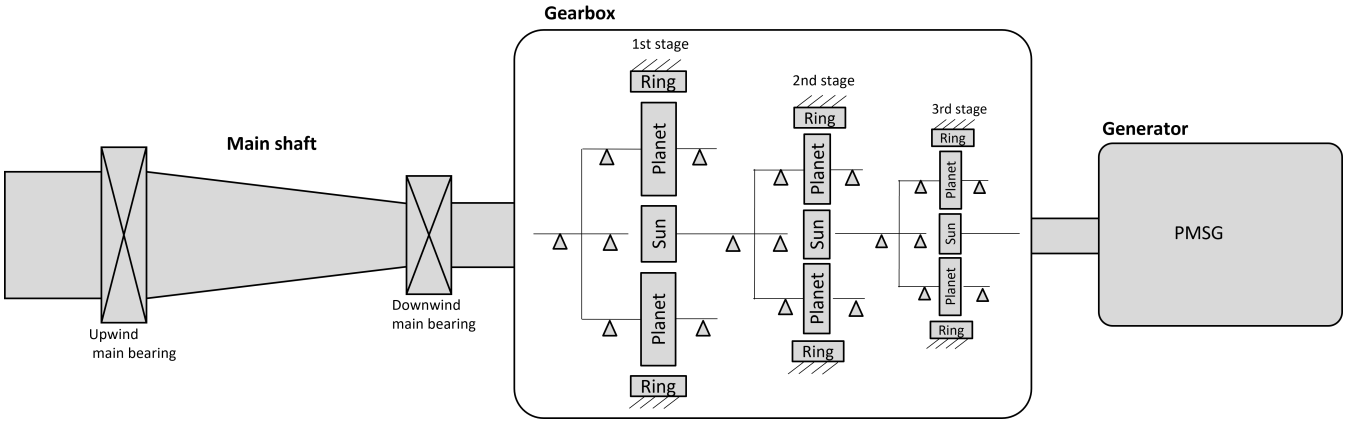

Figure 2. Drivetrain layout.

Evaluation metrics and benchmarking The case study pursues two main objectives: (i) to assess the robustness and efficiency of the proposed optimization framework and demonstrate its applicability within a system-level drivetrain design context, and (ii) to benchmark the optimized medium-speed drivetrain against the IEA 15 MW direct-drive reference system. The benchmarking focuses on comparisons of nacelle mass, efficiency, and reliability.

Table 4. Environmental conditions from the Utsira Nord site used for drivetrain design.

Operation	U_w **[m/s]**	H_s **[m]**	T_p **[s]**	$\Delta\theta$ **[deg]**
Normal	3	0.1	5.701	-5.83
	5	0.1	5.701	-7.26
	7	0.1	5.701	-8.55
	9	0.2	5.934	-9.71
	11	0.3	6.124	-10.75
	13	0.4	6.290	-11.68
	15	0.5	6.443	-12.52
	17	0.6	6.585	-13.28
	19	0.7	6.719	-13.96
	21	0.9	6.970	-14.58
	23	1.1	7.203	-15.13
	25	1.4	7.530	-15.62
Extreme (50-year)	37.5	14.4	16.157	-17.77
Extreme (1-year)	31.0	9.6	13.412	-16.83

https://doi.org/10.5194/wes-2026-90
Preprint. Discussion started: 17 June 2026

eawe european academy of wind energy
Open Access WIND ENERGY SCIENCE DISCUSSIONS

Table 5. Design load cases (DLCs) selected for the drivetrain design.

DLC	Wind condition	Wind speeds [m/s]	Additional settings	# of seeds	# of simulations
1.2	NTM	3:2:25	–	6	72
1.3	ETM	3:2:25	–	6	72
1.4	ECD	11	± Direction change	1	2
1.5	EWS	3:2:25	± Vertical/Horizontal shear	1	48
3.2	EOG	3, 11, 25	Start-up	1	12
3.3	EDC	3, 11, 25	Start-up, ± Direction change	1	24
4.2	EOG	11, 25	Shutdown	1	4
5.1	NTM	11, 25	Emergency stop	6	12
6.1	EWM	37.5	Yaw $\pm 8^\circ$	6	12
6.3	EWM	31	Yaw $\pm 15^\circ$	6	12

4 Discussion of results

The proposed framework is evaluated from three perspectives: (i) numerical fidelity relative to established industry tools (Sec. 4.1), (ii) optimization robustness and computational behavior (Sec. 4.34.4), and (iii) drivetrain-level design trade-offs and performance benefits. The following sections therefore progress from component-level validation toward system-level drivetrain analysis.

4.1 Validation against KISSsoft and WISDEM

Before assessing drivetrain-level optimization results, the proposed framework (MADE4WIND) must first be validated against established tools. Validation is performed at two complementary levels: (i) against KISSsoft for detailed component calculations, and (ii) against WISDEM for drivetrain-level stage-ratio allocation.

4.1.1 Validation against KISSsoft: calculation fidelity and optimization behaviour

KISSsoft provides industry-standard implementations for gear geometry, load distribution, ISO 6336 gear safety, efficiency, and component weight estimation. MADE4WIND implements equivalent analytical formulations based on ISO 6336, ISO 281, and DIN 743.

Table 6 presents a comparison of selected quantities for a representative planetary stage. Relative deviations are consistently small: geometric quantities deviate by less than 0.02%, gear forces by less than 0.001%, and safety factors typically by less than 1%. Shaft and bearing safety factors show deviations below 0.05%, and efficiency differs by only 0.017% in absolute terms.

The slightly larger discrepancies observed for root safety factors (up to $\approx 1.6\%$) are primarily attributed to differences in microgeometry assumptions, such as tip alteration and chamfering, which influence the form factor Y_F in ISO 6336-3. These

https://doi.org/10.5194/wes-2026-90
Preprint. Discussion started: 17 June 2026

eawe european academy of wind energy
Open Access WIND ENERGY SCIENCE DISCUSSIONS

features are treated differently in KISSsoft and are not fully parameterized in the current MADE4WIND implementation. Overall, the comparison confirms high-fidelity reproduction of KISSsoft reference calculations.

The optimization capability was evaluated for the first planetary stage of the 15 MW drivetrain with target ratio $i_{st} = 3.6741$, root and flank constraints ($SF > 1.56$, $SH > 1.25$), and objective of minimum stage weight. Table 7 compares the five best solutions from both tools.

MADE4WIND converges to designs in the same geometric region as KISSsoft (five planets, module 32 mm, comparable tooth number combinations), while achieving lower stage weights. The best MADE4WIND solution is 7.2% lighter than the best KISSsoft result.

This difference arises from the continuous-variable formulation in MADE4WIND, which allows convergence directly to active constraint limits. In contrast, KISSsoft's "Fine sizing macrogeometry" tool operates on a discretized search grid, preventing exact convergence to constraint boundaries. The comparison demonstrates that MADE4WIND reproduces KISSsoft calculations with high numerical accuracy while enabling more efficient continuous optimization.

4.2 Validation against WISDEM: system-level behaviour

At the system level, the proposed framework was benchmarked against NREL's WISDEM drivetrain sizing module for 15 MW medium-speed configurations with total gearbox ratios between 1:40 and 1:80. The comparison focuses on stage-ratio allocation.

Figure 3 compares the normalized stage ratios $(i_{st,k}/i_{gb}^{1/3})$ predicted by WISDEM and obtained from the MADE4WIND optimization. WISDEM exhibits a smooth, monotonic scaling behaviour: the first-stage share decreases with increasing total ratio, while the third stage carries an increasing fraction of the transmission. This reflects heuristic allocation rules derived from historical drivetrain data.

In contrast, MADE4WIND yields an adaptive and constraint-driven redistribution of the transmission ratio across the stages. The first-stage ratio remains consistently below the equal-ratio split, while the second and third stages absorb most of the variation in total gearbox ratio. This behavior emerges naturally from the coupled interaction of ISO 6336 gear strength constraints, ISO 281 bearing constraints, and DIN 743 shaft safety requirements, which follow different scaling laws with respect to transmitted torque. Gear root bending stresses scale approximately linearly with torque, $\sigma_F \sim T^1$, whereas Hertzian flank contact stresses follow a weaker relationship, $\sigma_H \sim T^{1/2}$. Bearing fatigue damage is substantially more sensitive, since the equivalent dynamic load follows relation $DEL \sim T^{10/3}$. Stages governed by bearing constraints therefore tend to receive a smaller share of the overall transmission ratio, while stages dominated primarily by flank contact constraints can accommodate larger ratio increases with comparatively smaller mass penalties. The resulting ratio distributions are therefore non-monotonic and emerge directly from the active constraint state of each stage rather than from proportional scaling assumptions.

The impact of this redistribution is quantified in Figure 4, which shows the relative mass difference. Across all investigated gearbox ratios, the MADE4WIND-optimized configurations are consistently lighter, achieving mass reductions of approximately 4–5% compared to WISDEM stage splits. The largest improvement occurs near $i_{gb} = 60$, where stress redistribution between stages is most effective.

https://doi.org/10.5194/wes-2026-90
Preprint. Discussion started: 17 June 2026

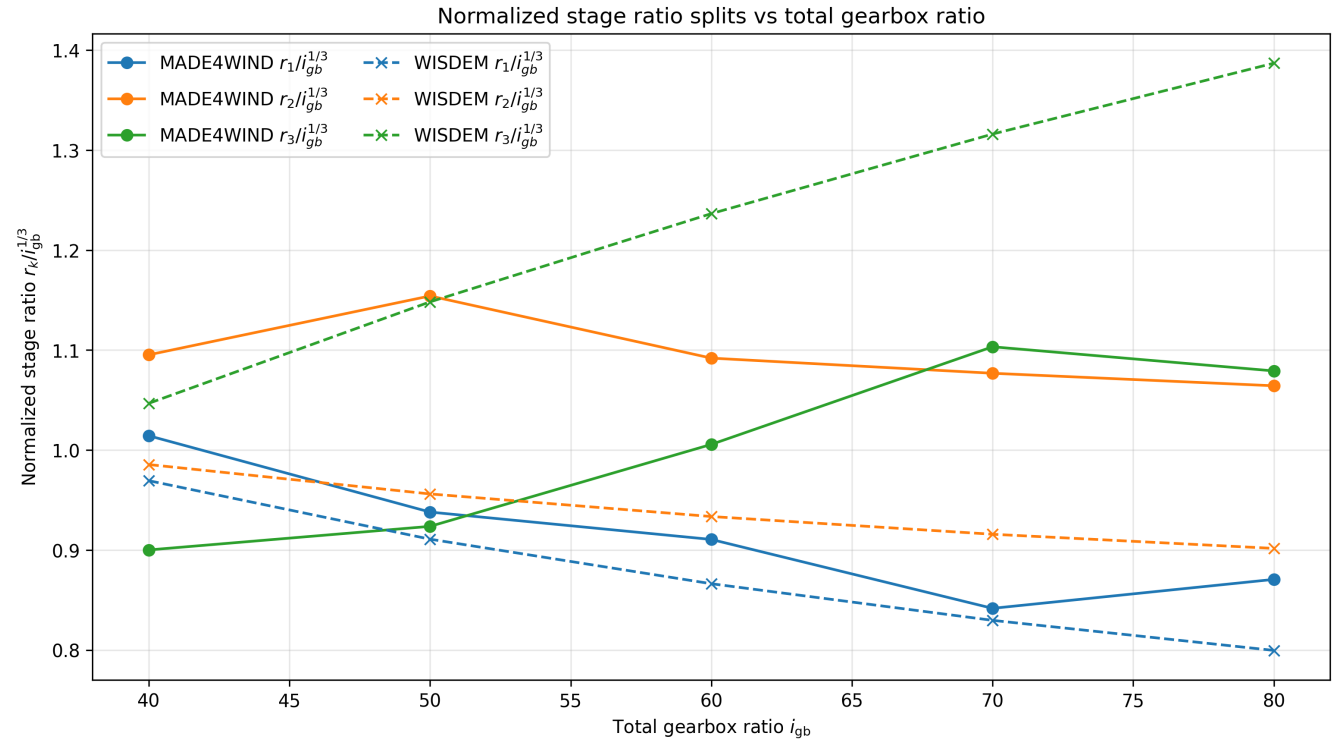

Figure 3. Normalized stage ratio distribution $(i_{st,k}/i_{gb}^{1/3})$ for the three planetary stages as a function of total gearbox ratio i_{gb}. Solid lines denote the MADE4WIND optimization results, while dashed lines represent WISDEM stage splits.

These results demonstrate that stage-ratio allocation should be treated as an integrated optimization variable rather than a heuristic scaling parameter. Even at fixed total gearbox ratio, physics-based redistribution of stage ratios yields systematic and non-negligible mass reductions while fully satisfying standards-based reliability constraints.

4.3 Problem landscape and solver suitability

The optimization problem exhibits fundamentally different structural characteristics at the continuous, discrete, and system levels. Understanding these landscape properties motivates the proposed hierarchical solver architecture.

4.3.1 Continuous stage-level landscape.

At the innermost layer, the design variables are continuous geometric parameters (e.g., face width, profile shifts, and overlap ratio) for a fixed discrete gear configuration. Figure 5 shows representative two-dimensional slices of this space. Feasibility is restricted to narrow regions defined by safety and geometric constraints; however, within these regions the objective function varies smoothly and exhibits well-defined gradients.

https://doi.org/10.5194/wes-2026-90
Preprint. Discussion started: 17 June 2026

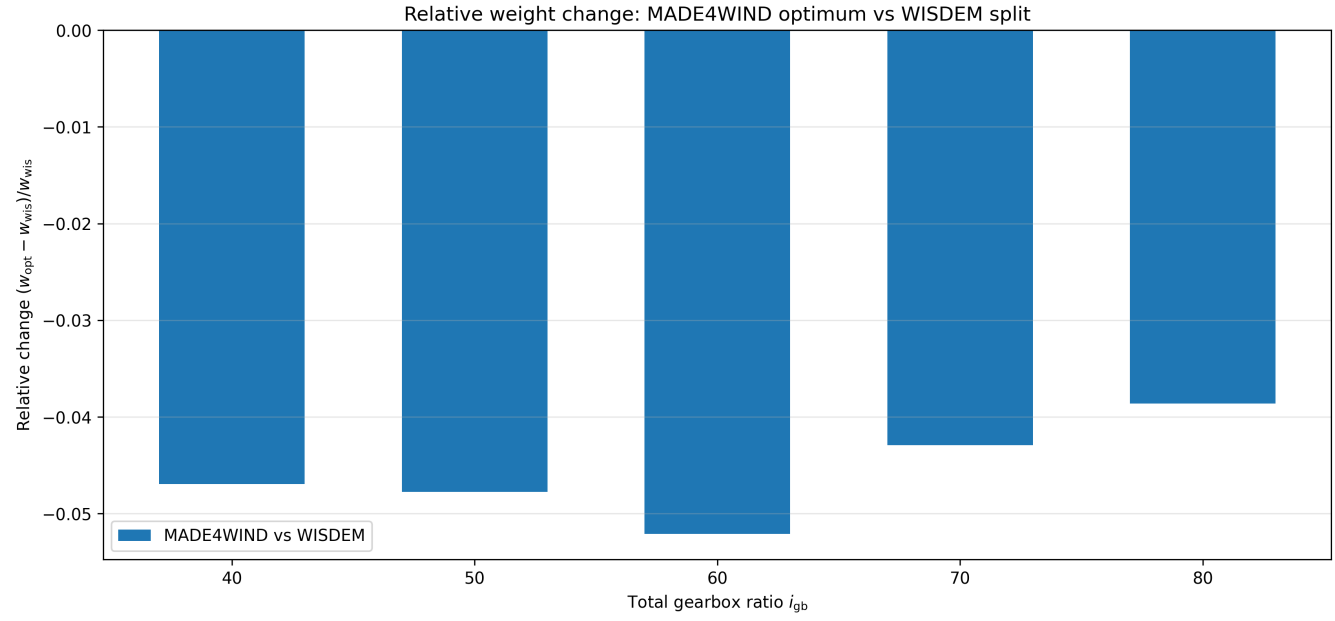

Figure 4. Relative drivetrain mass difference between the MADE4WIND-optimized stage ratio distribution and the WISDEM stage split as a function of total gearbox ratio i_{gb}.

This structure is well suited for gradient-based optimization: once a feasible basin is identified, rapid local convergence toward the active constraint boundaries is observed.

4.3.2 Discrete stage-level landscape.

At the intermediate layer, the design variables comprise discrete tooth numbers, normal modules, and planet counts. Figure 6 illustrates the objective distribution across all 560 feasible discrete candidates within the prescribed bounds. Although the design space is disconnected, clear global trends are visible. Distinct bands correspond to different normal modules, and weight generally increases with increasing tooth number combinations.

Despite the absence of continuity, the landscape is strongly structured by physics-based scaling laws. These global trends guide the search toward the global minimum region, making stochastic population-based methods such as Differential Evolution both robust and efficient at this layer.

4.3.3 System-level landscape.

At the outermost layer, the design variables are the stage ratios bounded by their prescribed variable limits. Within this bounded domain, the objective exhibits a clear global trend: balanced ratio distributions near the nominal equal split yield lower gearbox weight, whereas strongly unbalanced splits increase weight due to disproportionate torque loading and unfavorable gear scaling. However, the system-level landscape is not fully smooth. Since each stage internally selects discrete tooth numbers

https://doi.org/10.5194/wes-2026-90
Preprint. Discussion started: 17 June 2026

eawe european academy of wind energy
Open Access WIND ENERGY SCIENCE DISCUSSIONS

Table 6. Verification of selected drivetrain quantities against KISSsoft reference results. Relative error is given in percent.

Category	Parameter	KISSsoft	MADE4WIND	Rel. Error [%]
Geometry	x_r	-0.559000	-0.558917	0.0148
	a [mm]	1600.0000	1599.9988	0.0001
	$\varepsilon_{\alpha,t,sp}$	1.333000	1.332748	0.0189
	$\varepsilon_{\alpha,t,rp}$	1.394248	1.394000	0.0180
Loads	F_{rad} [N]	4 279 900	4 279 882.5	0.0004
	F_{ax} [N]	0.0000	0.0625	–
	F_t [N]	1 993 600	1 993 617.1	0.0009
Root safety	SF_s	2.4600	2.4819	0.8909
	SF_p	1.8900	1.8984	0.4427
	SF_r	3.1400	3.0899	1.5953
Flank safety	SH_s	1.5300	1.5310	0.0920
	SH_p	1.5700	1.5740	0.2760
	SH_r	2.7200	2.7250	0.1720
Shaft safety	$S_{\mathrm{ULS},p}$	37.1100	37.0975	0.0336
	$S_{\mathrm{ULS},s}$	1.1000	1.1000	0.0001
Bearing safety	SB	1.20909	1.209135	0.000037
Efficiency	η	0.9953	0.9951	0.0170

Table 7. Top-5 drivetrain designs from KISSsoft and MADE4WIND optimization. Minimum safety factors (SF/SH) are reported as the minimum across sun, planet, and ring gears.

Design	W	N_p	m_n [mm]	z_s	z_p	z_r	x_s	x_p	β [°]	b [mm]	a [mm]	$\mathrm{SF}_{\mathrm{min}}$	$\mathrm{SH}_{\mathrm{min}}$
KISSsoft #1	54932	5	32	41	33	109	-0.36056	0.18338	15.0	550.0	1220.0	1.79	1.27
KISSsoft #2	55663	5	32	41	35	109	-0.35307	-0.20449	15.0	550.0	1240.0	1.95	1.28
KISSsoft #3	55758	5	32	45	38	120	-0.12415	-0.02541	15.0	450.0	1370.0	1.61	1.30
KISSsoft #4	56878	5	32	41	34	109	-0.01187	0.25662	15.0	550.0	1250.0	1.67	1.31
KISSsoft #5	57214	5	32	40	31	105	0.29364	0.50433	15.0	600.0	1200.0	1.68	1.34
MADE4WIND #1	50974	5	32	40	32	105	0.12483	0.10815	12.8	546.2	1188.5	1.56	1.25
MADE4WIND #2	51144	5	32	43	34	112	-0.02947	-0.04182	14.5	482.0	1270.2	1.56	1.25
MADE4WIND #3	50913	5	32	38	31	102	0.24561	0.16889	11.9	583.7	1141.1	1.56	1.25
MADE4WIND #4	51357	5	32	38	32	102	0.16801	0.19768	12.1	575.5	1156.8	1.56	1.25
MADE4WIND #5	51588	5	32	41	34	109	0.00833	0.04401	13.7	508.4	1236.9	1.56	1.25

and modules, small variations in stage ratios may activate different discrete optima, resulting in local pockets and piecewise transitions in the aggregated objective.

https://doi.org/10.5194/wes-2026-90
Preprint. Discussion started: 17 June 2026

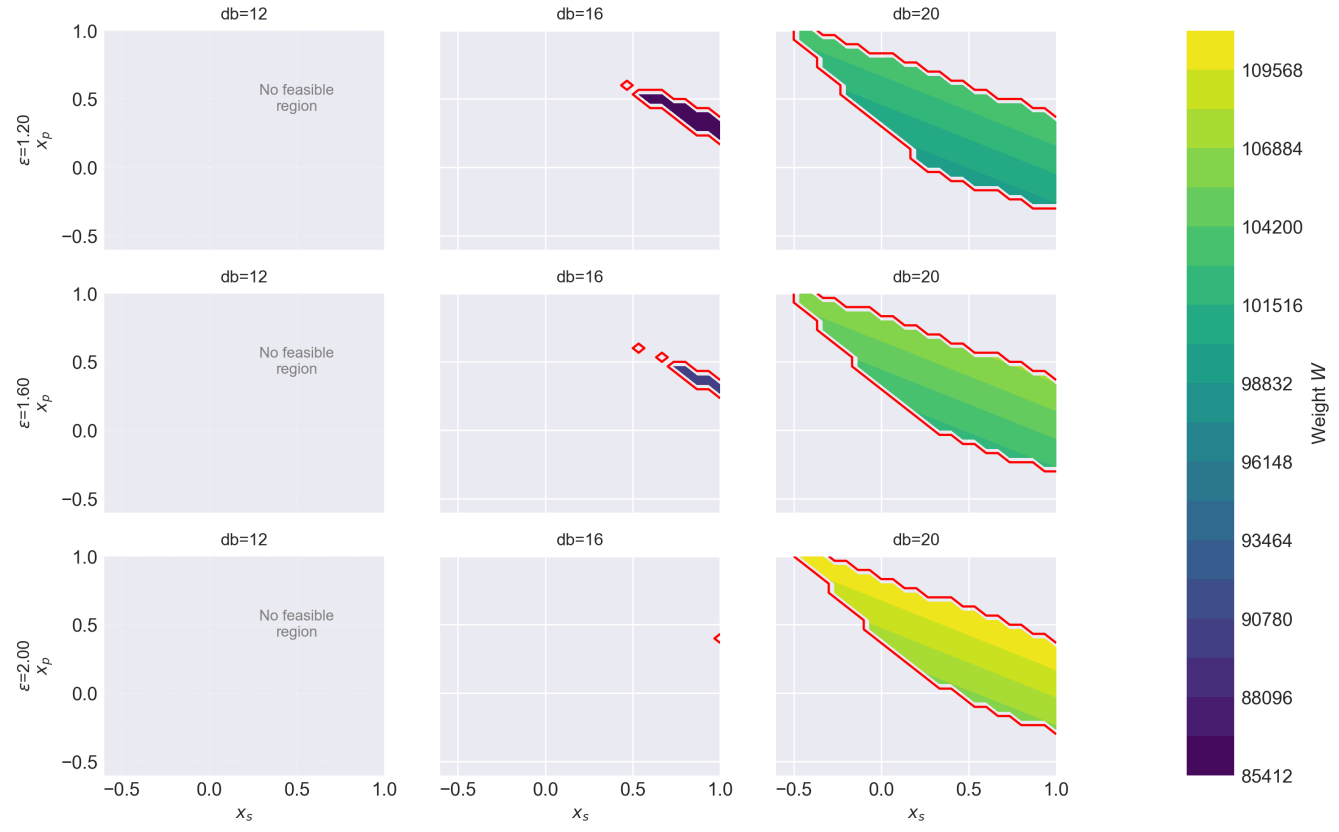

Figure 5. Continuous stage-level design landscape shown as two-dimensional slices of the objective function (stage weight). Feasible regions are bounded strength and geometric constraints (red contours).

4.3.4 Implications for solver design.

The overall optimization problem is therefore multi-level and mixed-integer with three distinct landscape structures: (i) smooth and differentiable continuous subproblems, (ii) structured but disconnected discrete search spaces, and (iii) a low-dimensional but piecewise-defined system-level landscape.

A monolithic optimization strategy would be inefficient or unreliable across all layers. Instead, the hierarchical approach exploits the structure at each level: stochastic global search efficiently explores the discrete and system-level spaces, guided by strong physics-driven trends, while gradient-based solvers rapidly converge within the smooth continuous subspaces.

https://doi.org/10.5194/wes-2026-90
Preprint. Discussion started: 17 June 2026

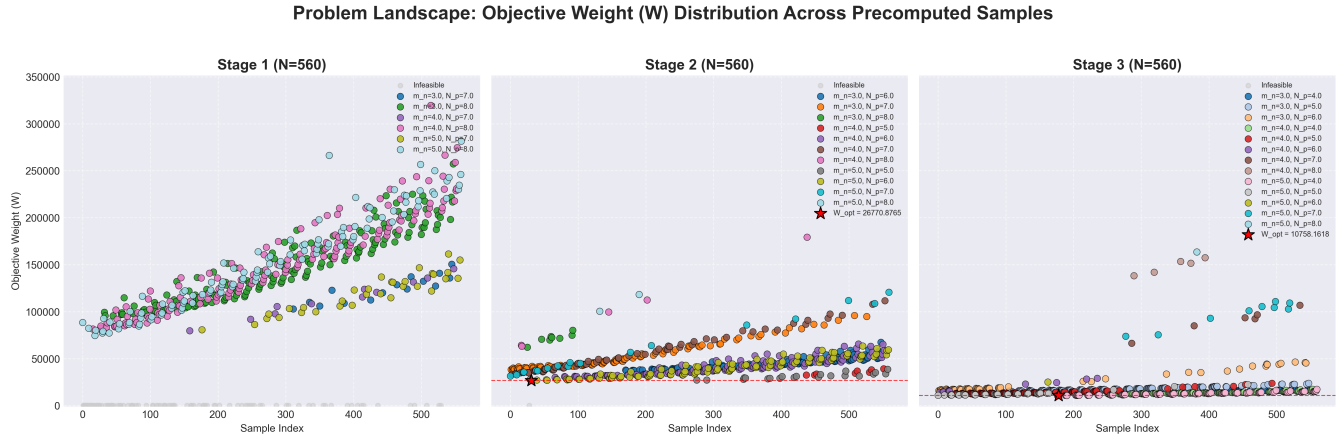

Figure 6. Discrete stage-level objective landscape for all feasible topology candidates within the prescribed bounds.

Table 8. Hyperparameter sweep settings for the three optimization layers. All studies used $N_{\text{samples}} = 128$ Latin Hypercube samples and $N_{\text{trials}} = 50$ repeated optimization runs per configuration.

Layer	Hyperparameter	Description	Range / setting	Sampling
Continuous refinement	I	Maximum optimizer iterations	$[10, 200]$	integer
	f_{tol}	Objective convergence tolerance	10^{-8}–10^{-4}	log-uniform
	g_{tol}	Constraint convergence tolerance	10^{-8}–10^{-4}	log-uniform
Discrete topology	P	Population size	$[10, 50]$	integer
	I	Maximum generations	$[1, 20]$	integer
	F	Mutation factor	$[0.5, 0.9]$	uniform
	C_r	Recombination rate	$[0.6, 1.0]$	uniform
Stage-ratio allocation	P	Population size	$[1, 10]$	integer
	I	Maximum generations	$[1, 10]$	integer
	F	Mutation factor	$[0.5, 0.9]$	uniform
	C_r	Recombination rate	$[0.6, 1.0]$	uniform

4.4 Convergence bevavior

4.4.1 Hyperparameter sweep

A structured hyperparameter sweep was conducted to evaluate the convergence behavior, solution quality, and computational cost of all three optimization layers of the proposed hierarchical framework. The investigated hyperparameter ranges are summarized in Table 8. All studies used 128 Latin Hypercube sampled configurations with 50 repeated optimization runs per configuration.

https://doi.org/10.5194/wes-2026-90
Preprint. Discussion started: 17 June 2026

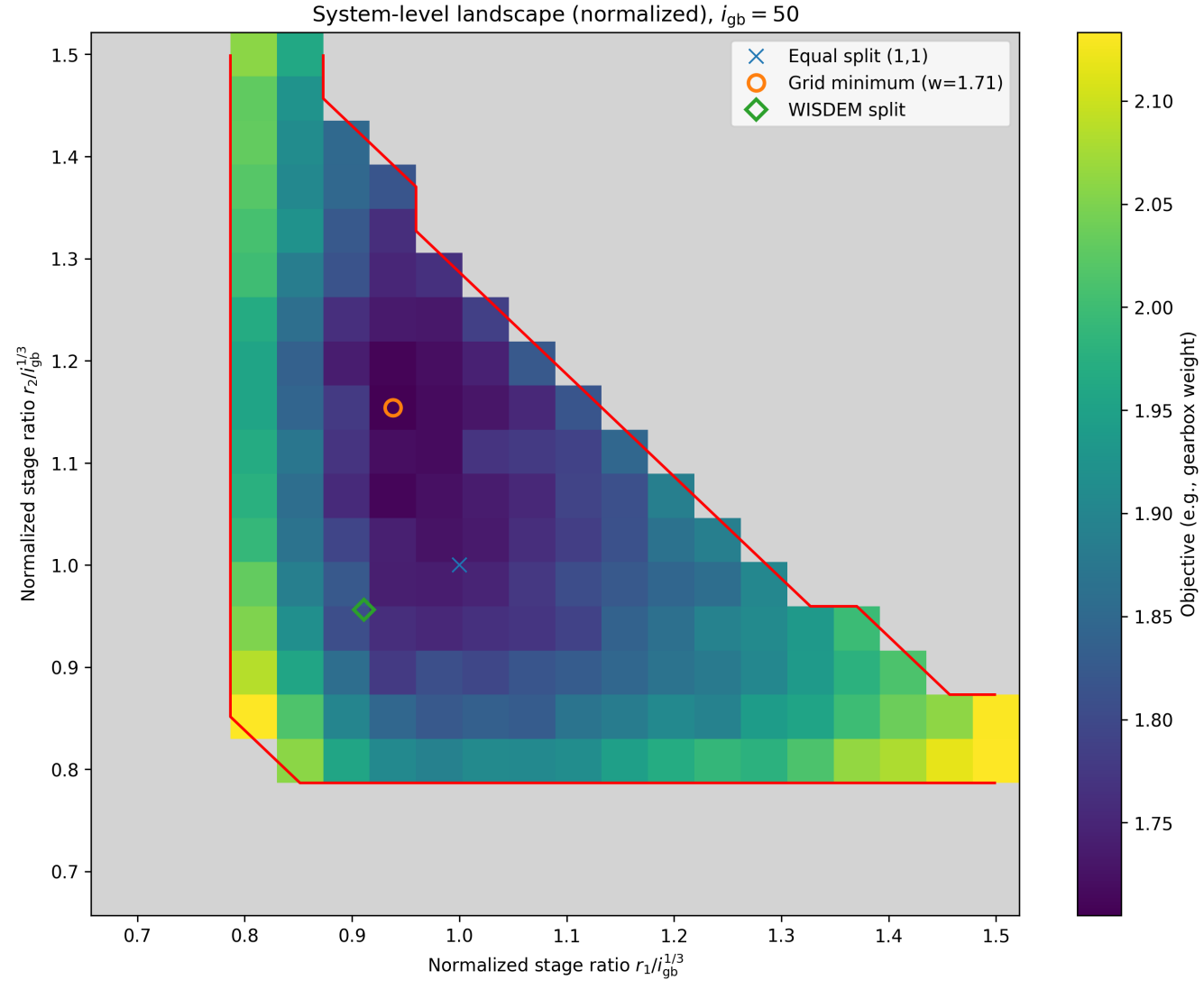

Figure 7. System-level gearbox weight landscape as a function of stage ratio distribution.

The inner continuous optimization layer was analyzed first using an LHS-based sweep of the SLSQP solver hyperparameters. Performance was evaluated in terms of mean objective deviation and average CPU time per solve. The convergence behavior of the continuous layer is shown in Fig. 8. The results reveal a clear asymptotic convergence trend: low-cost configurations converge rapidly but exhibit higher objective deviations, whereas moderate increases in CPU time significantly improve solution quality. Beyond approximately 0.5 s per optimization, further computational effort provides only limited improvement, indicating that the continuous optimization problem is comparatively well-conditioned once a feasible discrete topology

https://doi.org/10.5194/wes-2026-90
Preprint. Discussion started: 17 June 2026

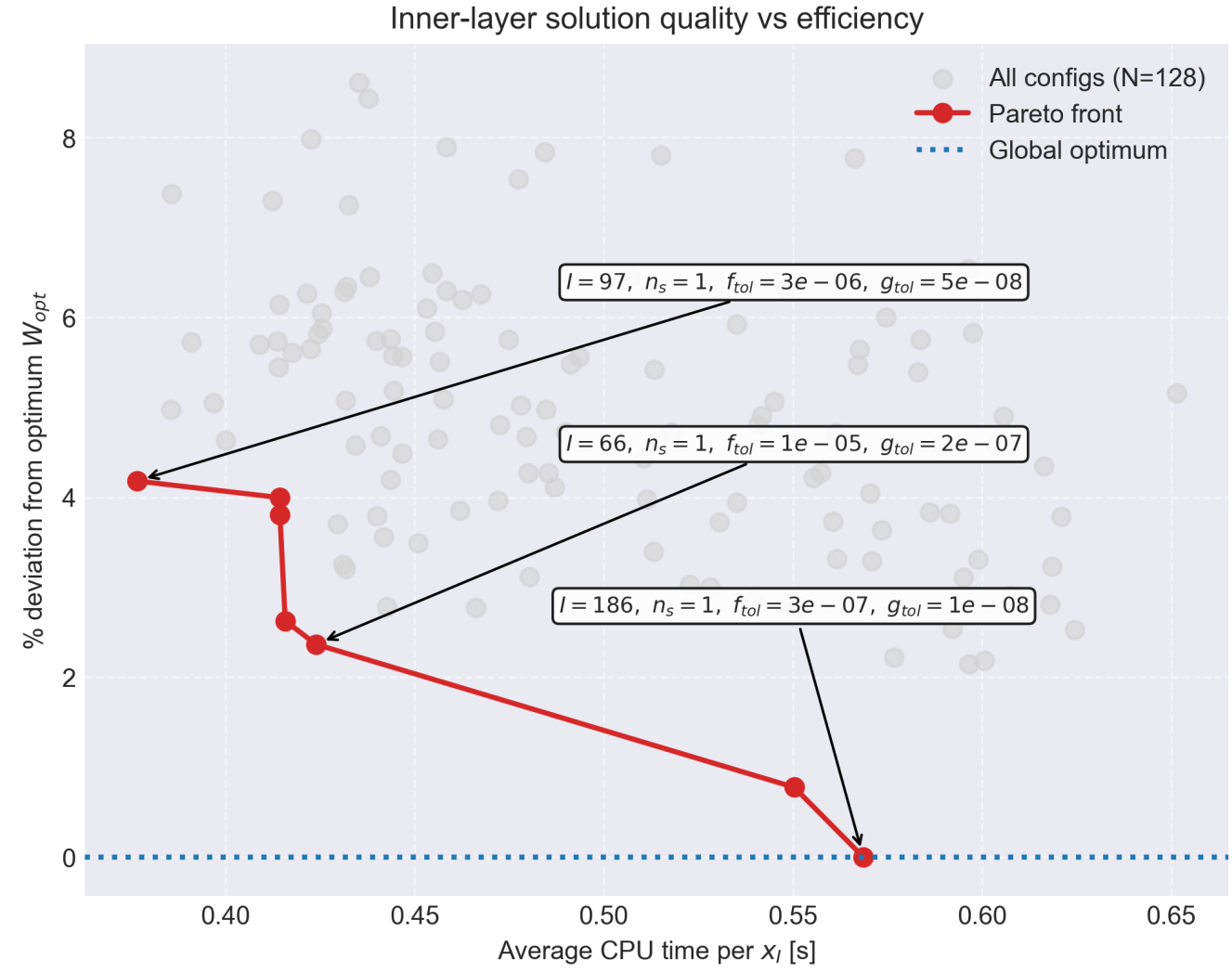

Figure 8. Inner-layer continuous optimization performance: mean objective value versus average CPU time per solve for 128 hyperparameter configurations.

has been identified. This behavior confirms that the differentiable reformulation and analytical gradients obtained through automatic differentiation enable highly efficient local convergence.

For the discrete stage-level optimization layer, Differential Evolution (DE) hyperparameters were investigated independently for all three gearbox stages. Figure 9 presents the resulting solution-quality versus computational-effort trade-off for the three stages. For all stages, the objective deviation decreases rapidly with increasing computational effort, indicating that the DE optimizer efficiently identifies the globally optimal region even at moderate function-evaluation (FE) budgets. Stage 1 exhibits the most challenging landscape, requiring approximately 150–250 FE to consistently achieve near-optimal solutions below

https://doi.org/10.5194/wes-2026-90
Preprint. Discussion started: 17 June 2026

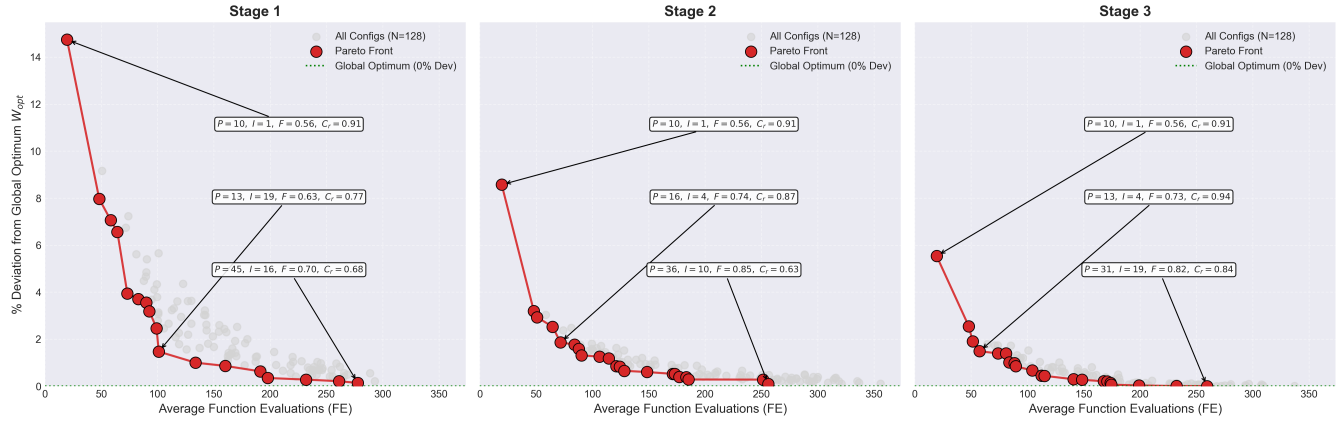

Figure 9. Discrete-layer solution quality as a function of computational effort.

1% deviation from the global optimum. Stages 2 and 3 converge more rapidly and typically achieve sub-percent deviations within approximately 100–200 FE. Beyond these ranges, additional function evaluations yield only marginal improvements, demonstrating diminishing returns in computational effort.

The outer gearbox-level optimization layer was evaluated using the same DE-based hyperparameter sweep strategy. Figure 10 shows the resulting relationship between solution quality and computational effort for the gearbox-level stage-ratio optimization. Similar to the discrete stage-level optimization, the objective deviation decreases rapidly with increasing FE budget. Near-optimal gearbox-level solutions are consistently obtained within approximately 20–40 FE, while larger evaluation budgets primarily improve robustness and reduce the probability of premature convergence to local minima.

4.4.2 Computational costs

The hyperparameter sweep additionally provides insight into the practical computational cost of the complete hierarchical optimization framework. The inner continuous optimization layer is computationally very efficient, requiring approximately 0.5 s per solve on a standard personal computer. Since the discrete stage-level optimization typically converges within approximately 200 FE, the optimization of a single gearbox stage requires roughly

$$200 \times 0.5\ \text{s} \approx 100\ \text{s}.$$

For a three-stage gearbox, the total stage-level optimization cost therefore lies in the range of approximately 100–300 s, depending on the degree of parallelization across stages. The outer gearbox-level optimization converges within approximately 30 FE, leading to a total optimization time of approximately

$$30 \times (100\text{–}300\ \text{s}) \approx 3000\text{–}9000\ \text{s},$$

corresponding to approximately 0.8–2.5 hours for a complete drivetrain synthesis and optimization on a conventional desktop computer.

https://doi.org/10.5194/wes-2026-90
Preprint. Discussion started: 17 June 2026

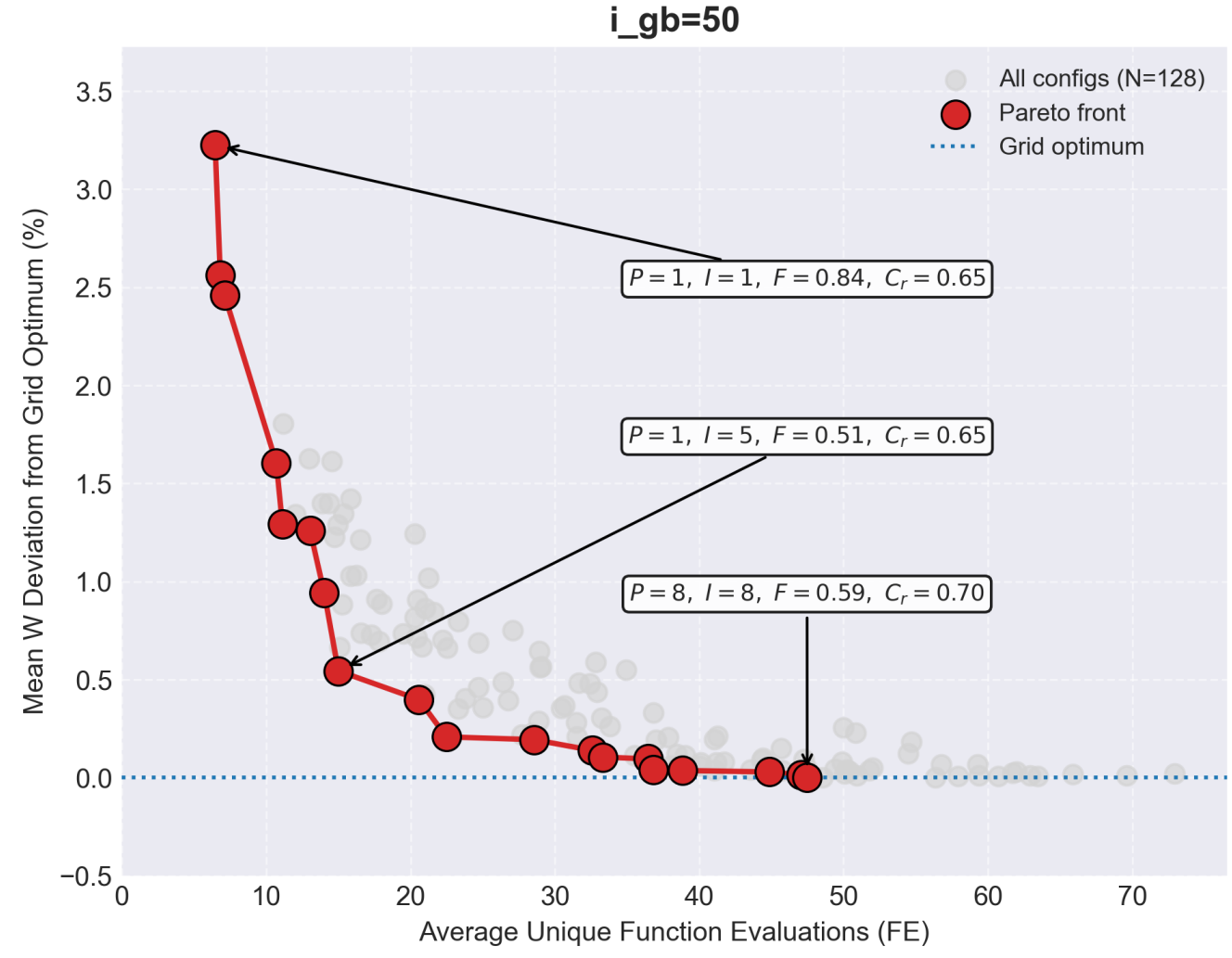

Figure 10. Outer-layer solution quality as a function of computational effort.

Overall, the convergence studies demonstrate that the proposed hierarchical framework achieves high-quality drivetrain solutions at practical computational cost.

4.5 System-level optimization analysis

Having validated the numerical fidelity and optimization robustness of the proposed framework, the methodology is then applied to investigate system-level drivetrain trade-offs. The analysis focuses on three aspects: the mass–efficiency trade-off, the optimization of gear stage numbers and total transmission ratios, and the resulting performance relative to the IEA 15

https://doi.org/10.5194/wes-2026-90
Preprint. Discussion started: 17 June 2026

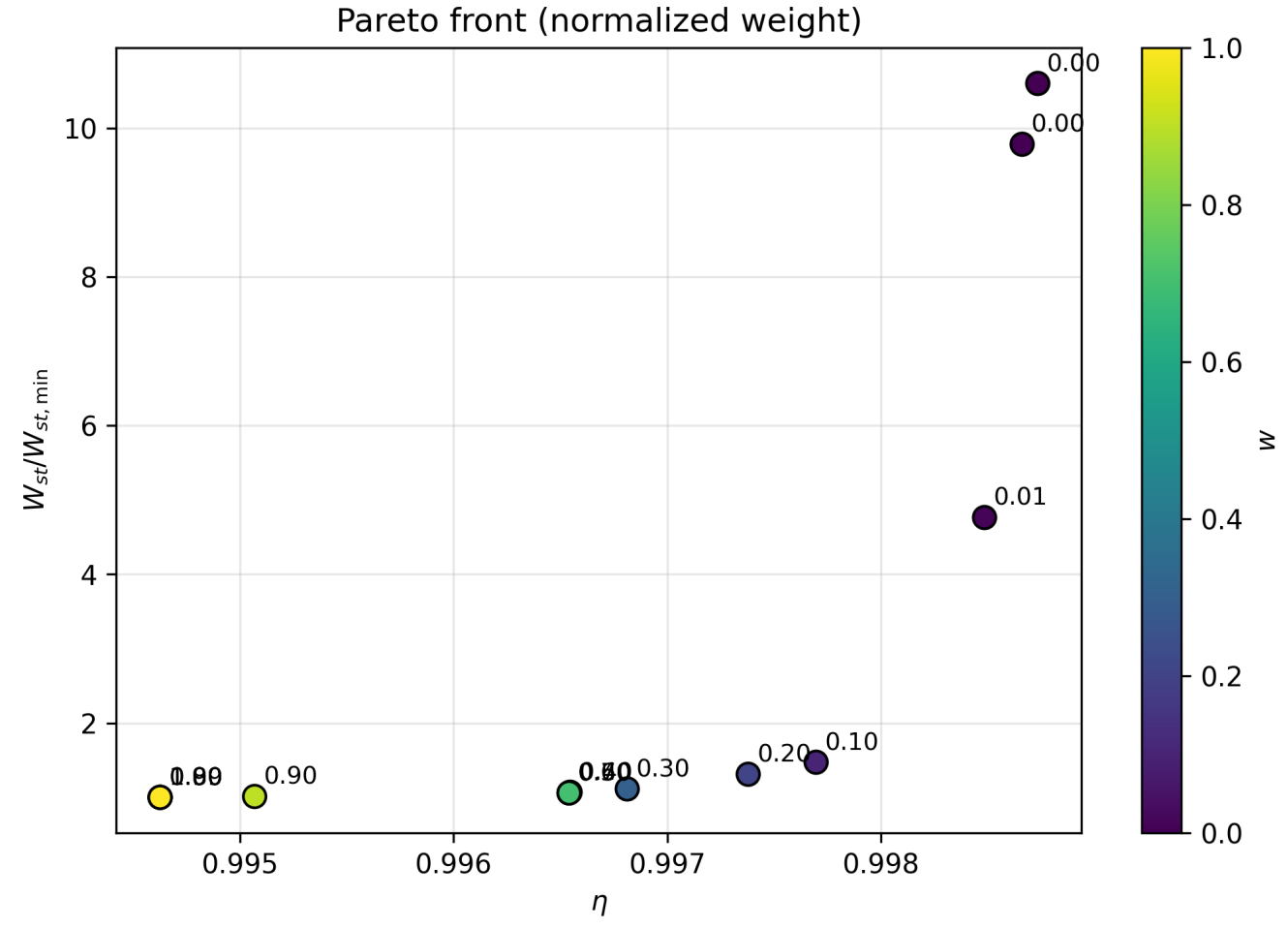

Figure 11. Pareto front of normalized drivetrain mass versus efficiency obtained by varying the weighting parameter w in the scalarized objective function.

MW direct-drive reference. Together, these studies demonstrate how integrated hierarchical optimization enables informed architecture selection for next-generation offshore wind turbine drivetrains.

4.5.1 Mass–efficiency trade-off

The multi-objective formulation reveals a clear trade-off between drivetrain mass and efficiency. Figure 11 presents the Pareto front obtained by varying the weighting parameter w in the scalarized objective function. The horizontal axis shows drivetrain efficiency η, while the vertical axis represents normalized drivetrain mass relative to the minimum achievable mass solution.

https://doi.org/10.5194/wes-2026-90
Preprint. Discussion started: 17 June 2026

As expected, configurations optimized purely for efficiency ($w \to 0$) achieve the highest efficiencies but at a significant mass penalty. These solutions typically favor lower gear loading and larger geometric safety margins, resulting in increased module sizes, face widths, and bearing dimensions. Consequently, drivetrain mass rises sharply as efficiency approaches its upper limit.

Conversely, solutions optimized primarily for mass ($w \to 1$) reduce gearbox dimensions and structural margins, leading to lighter designs but with slightly reduced efficiency due to higher contact forces and increased mesh losses.

The Pareto front exhibits a distinctly non-linear shape. In the intermediate region ($w \approx 0.3$–0.6), small reductions in efficiency yield disproportionately large mass savings. However, beyond a certain efficiency threshold ($\eta \gtrsim 0.998$), further efficiency improvements result in rapidly increasing mass. This indicates diminishing returns near the high-efficiency limit, where incremental reductions in mesh loss require substantial increases in gear size and structural stiffness.

The selected reference design lies within the knee region of the Pareto front, balancing mass and efficiency.

4.5.2 Architecture-level drivetrain trade-off analysis

To demonstrate the capability of the framework to perform drivetrain-level architecture optimization, a parametric study was conducted over gearbox ratios and number of stages. For each configuration, the hierarchical gearbox optimization was executed and coupled to a generator scaling model, allowing evaluation of the total drivetrain mass. The generator mass estimates were provided by the project partner INDAR, who extrapolated from a proven 8 MW permanent-magnet synchronous generator (PMSG) design using similarity laws.

Figure 12 illustrates the optimized generator and gearbox masses for two-, three-, and four-stage configurations across gearbox ratios between 1:40 and 1:80.

Increasing the gearbox ratio reduces generator mass by lowering the torque at the generator shaft. However, this effect is partially offset by increasing gearbox mass, particularly in two-stage configurations where elevated gear loads lead to larger modules and face widths.

The three-stage configuration provides the most favorable trade-off, maintaining an approximately constant gearbox mass across the investigated ratio range while benefiting from the reduction in generator mass. The four-stage configuration remains heavier at lower ratios and only approaches the three-stage solution at higher ratios, reflecting diminishing returns from additional stages.

Importantly, this result emerges from the coupled drivetrain optimization rather than isolated component sizing. The optimal architecture therefore depends on the interaction between gearbox geometry, load distribution, and generator torque scaling.

4.5.3 Drivetrain performance and benchmarking

The optimized 15 MW medium-speed drivetrain was benchmarked against the IEA 15 MW direct-drive reference turbine to assess the performance gains enabled by the proposed multi-objective optimization framework. Figure 13 compares the mass distribution of the two drivetrains.

A three-stage planetary gearbox solution with a total gearbox ratio of 1:50 and optimized stage-ratio splits of $[3.456,\ 4.252,\ 3.403]$ was obtained. The optimized drivetrain achieves a total mass of 274.2 t, representing a 31.5 % reduction relative to the 400 t

https://doi.org/10.5194/wes-2026-90
Preprint. Discussion started: 17 June 2026

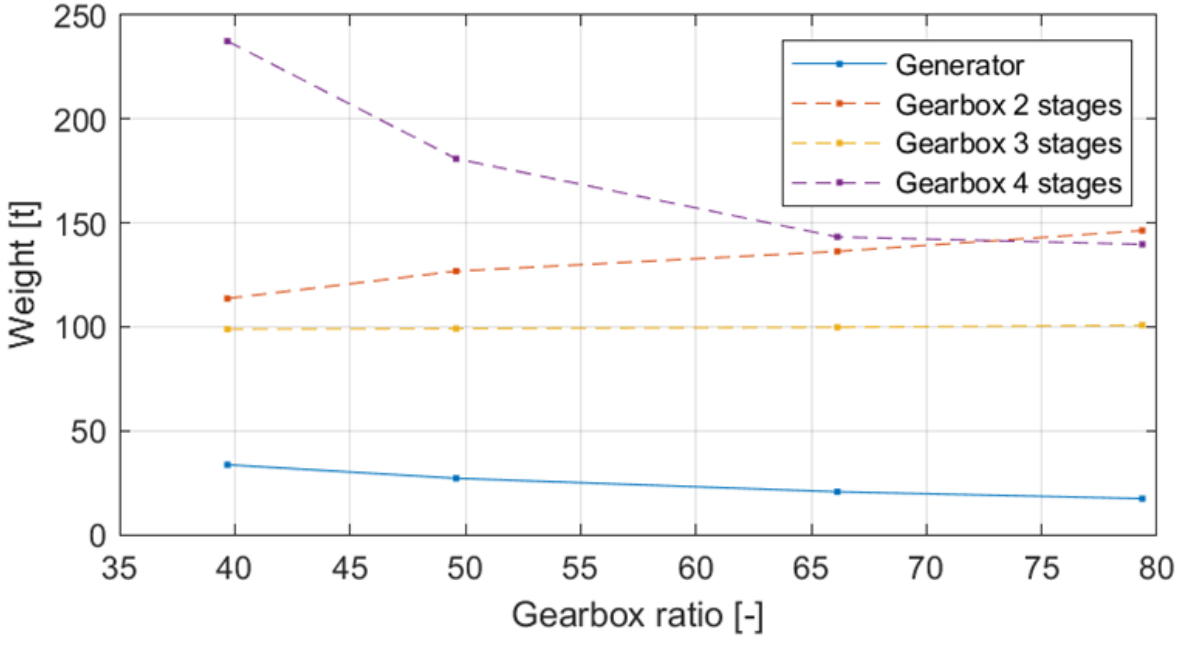

Figure 12. Architecture-level trade-off study: optimized generator and gearbox masses for two-, three-, and four-stage configurations across varying gearbox ratios.

direct-drive reference. The primary mass reduction arises from replacing the large-diameter direct-drive generator with a medium-speed gearbox coupled to a permanent-magnet synchronous generator (PMSG).

390 The optimized gearbox contributes 135.5 t and consists of three compact planetary stages synthesized through the hierarchical optimization procedure. The main shaft assembly weighs 120.7 t and incorporates cylindrical and tapered roller bearings designed to accommodate thrust and bending loads while mechanically isolating the gearbox from non-torque loading. Although the shaft is larger than in the direct-drive reference concept, this increase is offset by the substantial reduction in generator mass.

https://doi.org/10.5194/wes-2026-90
Preprint. Discussion started: 17 June 2026

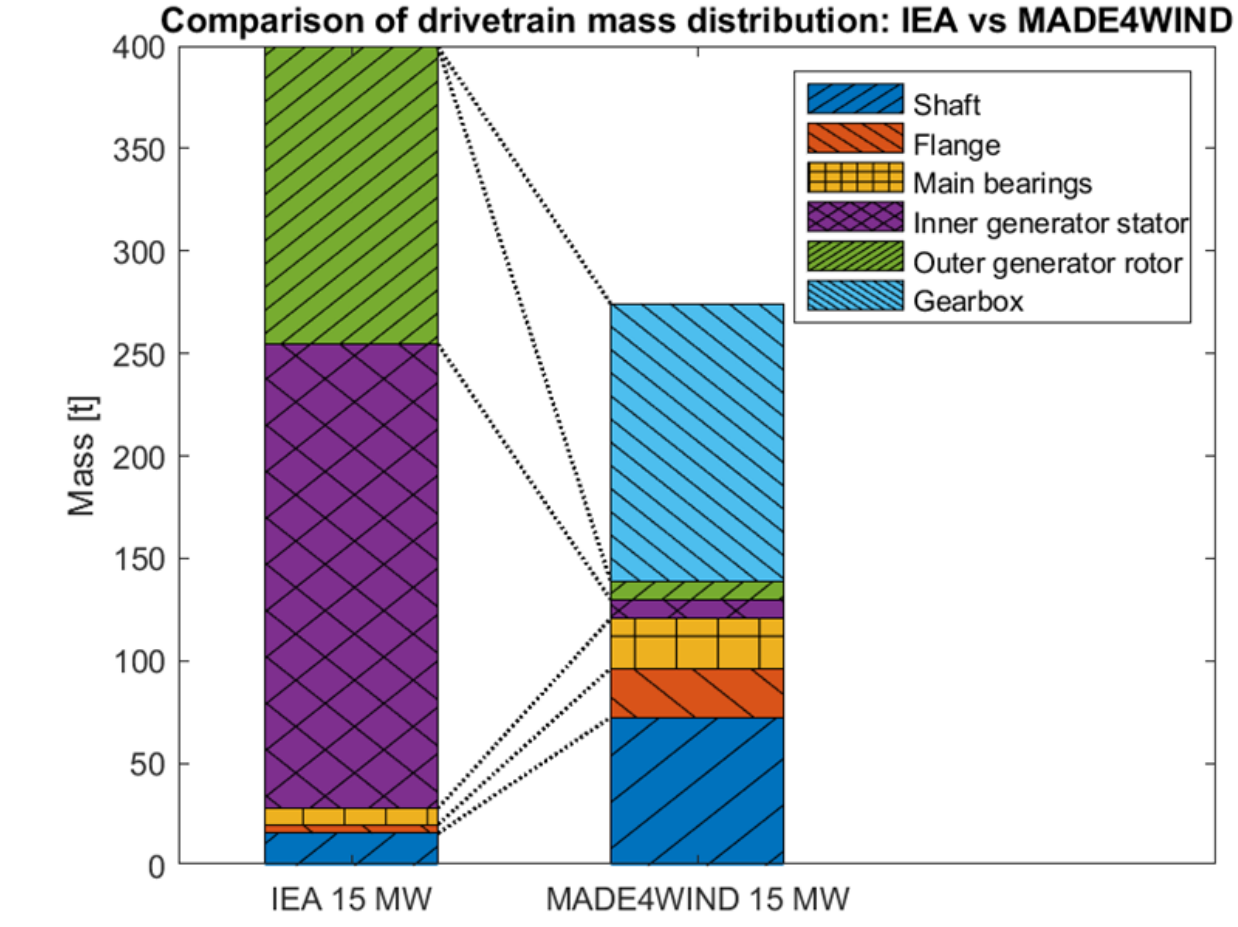

Figure 13. Benchmark comparison of drivetrain mass between the IEA 15 MW direct-drive reference and the optimized 15 MW medium-speed drivetrain.

The gearbox efficiency is 99.2 %, and when combined with a generator efficiency of 98.0 %, the overall drivetrain efficiency reaches 97.2 %. This is comparable to the 97.0 % efficiency of the direct-drive reference system, demonstrating that the mass reduction is achieved without compromising energy conversion performance.

From a structural perspective, the reduction in nacelle and overhang mass directly lowers tower-top loading and floating platform excitation. Preliminary system-level analyses indicate reduced pitch response and lower mooring line tensions for floating configurations, highlighting the broader system-level benefits of integrated drivetrain optimization.

https://doi.org/10.5194/wes-2026-90
Preprint. Discussion started: 17 June 2026

eawe european academy of wind energy
Open Access WIND ENERGY SCIENCE DISCUSSIONS

5 Conclusions

This work presented an open-access hierarchical optimization framework for the integrated design of medium-speed offshore wind turbine drivetrains. The proposed methodology combines mixed-integer architecture exploration with continuous gradient-based refinement, enabling simultaneous optimization of gearbox topology, stage-ratio distribution, gear geometry, shaft sizing, and bearing selection within a unified standards-based framework. By enforcing ISO 6336, ISO 281, and DIN 743 constraints in a fully differentiable formulation, the framework enables robust and computationally efficient gradient-based optimization using automatic differentiation.

Validation against KISSsoft demonstrated high numerical fidelity for geometry, loading, safety factors, and efficiency calculations. In addition, the continuous-variable optimization strategy consistently achieved lighter gearbox solutions than KISSsoft's discretized macrogeometry optimization workflow. For the investigated planetary stage, the optimized MADE4WIND solutions were approximately 7.2% lighter while satisfying the same standards-based safety constraints.

Benchmarking against WISDEM further highlighted the importance of treating stage-ratio allocation as an integrated optimization variable rather than relying on heuristic scaling rules. By optimizing the transmission-ratio distribution across the planetary stages under coupled ISO 6336, ISO 281, and DIN 743 constraints, the framework achieved systematic drivetrain mass reductions of approximately 4–5% relative to WISDEM stage splits across the investigated gearbox ratios.

The convergence studies demonstrated that the proposed hierarchical optimization strategy achieves high-quality drivetrain solutions at practical computational cost. A complete three-stage gearbox synthesis and optimization required approximately 0.8–2.5 hours on a conventional desktop computer.

The 15 MW case study demonstrated the capability of the framework to perform drivetrain-level synthesis and architecture trade-off analysis. A three-stage planetary gearbox solution with a total gearbox ratio of 1:50 and optimized stage-ratio splits of [3.456, 4.252, 3.403] was obtained. The optimized medium-speed drivetrain achieved a total nacelle mass of 274.2 t, corresponding to a 31.5% reduction compared to the direct-drive reference concept, while maintaining a competitive overall drivetrain efficiency of 97.2%, compared to 97.0% for the direct-drive configuration. Although the majority of the mass reduction originates from the technology shift from direct-drive to geared medium-speed architecture, the results demonstrate that the proposed optimization framework is capable of delivering highly competitive drivetrain solutions through integrated architecture and component optimization.

Overall, the results demonstrate that integrated, physics-based drivetrain synthesis is a powerful approach for next-generation offshore wind turbine design, particularly for floating applications where nacelle mass strongly influences structural loading and platform dynamics. Beyond the presented wind turbine application, the framework is general and transferable to gearbox design problems in other industries. The open-access implementation additionally provides a transparent and extensible foundation for future academic and industrial drivetrain optimization research.

https://doi.org/10.5194/wes-2026-90
Preprint. Discussion started: 17 June 2026

eawe european academy of wind energy
Open Access WIND ENERGY SCIENCE DISCUSSIONS

. **Code availability:** The complete source code for the drivetrain optimization framework developed in this work is openly available at: https://github.com/FelixMehlan/MADE4WIND-drivetrain-optimizer/

. **Author contributions** Felix C. Mehlan: Conceptualization, methodology, software development, validation, formal analysis, investigation, visualization, writing – original draft preparation.

435 Amir R. Nejad: Funding acquisition, supervision, review and editing.

. **Competing interest** Amir R. Nejad is a member of the editorial board of Wind Energy Science.

. **Acknowledgements** AI tools were used to assist with code development support and manuscript editing. All technical content, methodology development, implementation, analysis, validation, and scientific conclusions were developed and verified by the authors. The authors take full responsibility for the accuracy and integrity of the manuscript.

https://doi.org/10.5194/wes-2026-90
Preprint. Discussion started: 17 June 2026

eawe european academy of wind energy
Open Access WIND ENERGY SCIENCE DISCUSSIONS

Table A1. Factors for flank and root safety calculation

Factor	Symbol	Sun		Planet		Ring
Application factor	K_{A}	1.25		1.25		1.25
Mesh load factor	K_{γ}	1.1		1.1		1.1
Dynamic factor	K_{V}	1.0		1.0		1.0
Face load factor (flank)	$K_{\mathrm{H}\beta}$		1.18		1.04	
Transverse load factor (flank)	$K_{\mathrm{H}\alpha}$		1.0		1.0	
Face load factor (root)	$K_{\mathrm{F}\beta}$		1.20		1.04	
Transverse load factor (root)	$K_{\mathrm{F}\alpha}$		1.0		1.0	
Stress correction factor	Y_{ST}	2.0		2.0		2.0
Life factor	Y_{NT}			calc.		
Notch sensitivity factor	$Y_{\delta\mathrm{relT}}$	1.004		1.004		1.004
Relative surface factor	Y_{RrelT}	0.957		0.957		0.957
Alternate bending factor	Y_{M}	1.0		0.7		1.0
Size factor	Y_{X}			calc.		
Form factor	Y_{F}			calc.		
Stress correction factor	Y_{S}			calc.		
Helix angle factor	Y_{β}			calc.		
Rim thickness factor	Y_{B}	1.0		1.0		1.0
Deep tooth factor	Y_{DT}	1.0		1.0		1.0
Life factor	Z_{NT}			calc.		
Lubricant factor	Z_{L}	1.02		1.02		1.02
Velocity factor	Z_{V}	0.961		0.961		0.961
Roughness factor	Z_{R}			calc.		
Material hardening factor	Z_{W}	1.0		1.0		1.0
Size factor	Z_{X}	1.0		1.0		1.0
Contact factor	$Z_{\mathrm{B/D}}$	1.095		1.095		1.095
Zone factor	Z_{H}			calc.		
Elasticity factor	Z_{E}	189.8		189.8		189.8
Contact ratio factor	Z_{ϵ}			calc.		
Helix angle factor	Z_{β}	1.008		1.008		1.008

https://doi.org/10.5194/wes-2026-90
Preprint. Discussion started: 17 June 2026

eawe european academy of wind energy
Open Access WIND ENERGY SCIENCE DISCUSSIONS

Table A2. Polynomial coefficients for second-order bearing catalog curve fits. All functions follow the form $f(D,B) = p_{00} + p_{10}D + p_{01}B + p_{20}D^2 + p_{11}DB + p_{02}B^2$, with D and B in mm.

Parameter	p_{00}	p_{10}	p_{01}	p_{20}	p_{11}	p_{02}
C_1	131.8	-2.066	-0.5334	-0.004363	0.0992	-0.04296
d	-7.198	0.772	-0.3018	1.057×10^{-4}	-4.265×10^{-5}	-3.866×10^{-4}
X_1	1.0	-2.335×10^{-19}	1.787×10^{-19}	0	0	0
Y_1	1.634	1.997×10^{-4}	1.115×10^{-4}	0	0	0
W	42.95	-0.1774	-0.6657	-1.364×10^{-5}	0.003067	4.722×10^{-4}

Appendix A: Appendix

A1 Gear geometry

The detailed gear geometry is defined by the primary gear design variables, namely the tooth numbers z_1, z_2, z_3, normal module m_n, profile shift coefficients x_1, x_2, gear facewidth b, overlap ratio ϵ_δ and number of planets N_P. Auxiliary variables including pitch, root and tip diameters, center distance, helix angle and working pressure angle are calculated from geometric relations. First, the pitch diameters of the sun, planet, and ring gears are computed as:

$$d_{\mathrm{p},1} = \frac{z_1 m_\mathrm{n}}{\cos(\beta)}, \quad d_{\mathrm{p},2} = \frac{z_2 m_\mathrm{n}}{\cos(\beta)}, \quad d_{\mathrm{p},3} = \frac{z_3 m_\mathrm{n}}{\cos(\beta)}, \tag{A1}$$

where z_1, z_2, and z_3 are the numbers of teeth in the sun, planet, and ring gears, respectively. The helix angle β is defined by the overlap ratio ϵ_δ:

$$\beta = \arcsin\left(\epsilon_\delta \frac{\pi m_n}{b}\right) \tag{A2}$$

The transverse pressure angle α_t is calculated as:

$$\alpha_t = \arctan\left(\frac{\tan(\alpha_\mathrm{n})}{\cos(\beta)}\right), \tag{A3}$$

where α_n is the normal pressure angle. The base diameters of the sun, planet, and ring gears are given by:

$$d_{\mathrm{b},1} = d_{\mathrm{p},1}\cos(\alpha_t), \tag{A4}$$

$$d_{\mathrm{b},2} = d_{\mathrm{p},2}\cos(\alpha_t), \tag{A5}$$

$$d_{\mathrm{b},3} = d_{\mathrm{p},3}\cos(\alpha_t). \tag{A6}$$

The working tangential pressure angle $\alpha_{\mathrm{wt},12}$ is determined by solving the equation:

$$\mathrm{inv}(\alpha_{\mathrm{wt},12}) = 2\tan(\alpha_\mathrm{n})\frac{x_1 + x_2}{z_1 + z_2} + \mathrm{inv}(\alpha_\mathrm{t}), \tag{A7}$$

where x_1 and x_2 are the profile shift coefficients of the sun and planet gears, respectively.

https://doi.org/10.5194/wes-2026-90
Preprint. Discussion started: 17 June 2026

eawe european academy of wind energy
Open Access WIND ENERGY SCIENCE DISCUSSIONS

The working pitch diameters of the sun and planet gears are:

$$d_{\mathrm{pw},1} = \frac{d_{\mathrm{b},1}}{\cos(\alpha_{\mathrm{wt},12})}, \quad d_{\mathrm{pw},2} = \frac{d_{\mathrm{b},2}}{\cos(\alpha_{\mathrm{wt},12})}. \tag{A8}$$

The center distance modification coefficient y_{12} and the axis distance a are calculated as:

$$y_{12} = \frac{z_1 + z_2}{2}\left(\frac{\cos(\alpha_t)}{\cos(\alpha_{\mathrm{wt},12})} - 1\right), \tag{A9}$$

$$a = \left(\frac{z_1 + z_2}{2} + y_{12}\right)\frac{m_{\mathrm{n}}}{\cos(\beta)}. \tag{A10}$$

The working pitch diameter of the ring gear is:

$$d_{\mathrm{pw},3} = \frac{2a\,z_3}{z_3 - z_2}. \tag{A11}$$

The working tangential pressure angle $\alpha_{\mathrm{wt},23}$ for the ring-planet contact is:

$$\alpha_{\mathrm{wt},23} = \arccos\left(\frac{d_{\mathrm{b},3}}{d_{\mathrm{pw},3}}\right). \tag{A12}$$

The profile shift coefficient of the ring gear x_3 is given by:

$$x_3 = \frac{\mathrm{inv}(\alpha_t) - \mathrm{inv}(\alpha_{\mathrm{wt},23})}{2\tan(\alpha_{\mathrm{n}})}(z_3 - z_2) - x_2, \tag{A13}$$

The tip diameters of the sun, planet, and ring gears are:

$$d_{\mathrm{a},1} = d_{\mathrm{p},1} + 2(1 + x_1)m_{\mathrm{n}}, \tag{A14}$$

$$d_{\mathrm{a},2} = d_{\mathrm{p},2} + 2(1 + x_2)m_{\mathrm{n}}, \tag{A15}$$

$$d_{\mathrm{a},3} = d_{\mathrm{p},3} - 2(1 + x_3)m_{\mathrm{n}}. \tag{A16}$$

The root diameters of the sun, planet, and ring gears are:

$$d_{\mathrm{f},1} = d_{\mathrm{a},1} - 2(h_{\mathrm{a}} + h_{\mathrm{f}})m_{\mathrm{n}}, \tag{A17}$$

$$d_{\mathrm{f},2} = d_{\mathrm{a},2} - 2(h_{\mathrm{a}} + h_{\mathrm{f}})m_{\mathrm{n}}, \tag{A18}$$

$$d_{\mathrm{f},3} = d_{\mathrm{a},3} + 2(h_{\mathrm{a}} + h_{\mathrm{f}})m_{\mathrm{n}}. \tag{A19}$$

The inner diameter of the sun gear, the inner diameter of the planet gear, and the outer diameter of the ring gear are:

$$d_{\mathrm{i},1} = d_{\mathrm{f},1} - 2s_{\mathrm{R},1}m_{\mathrm{n}}, \tag{A20}$$

$$d_{\mathrm{i},2} = d_{\mathrm{f},2} - 2s_{\mathrm{R},2}m_{\mathrm{n}}, \tag{A21}$$

$$d_{\mathrm{o},3} = d_{\mathrm{f},3} + 2s_{\mathrm{R},3}m_{\mathrm{n}}, \tag{A22}$$

where $s_{\mathrm{R},1}$, $s_{\mathrm{R},2}$, and $s_{\mathrm{R},3}$ are the rim thickness coefficients for the sun, planet, and ring gears, respectively.

https://doi.org/10.5194/wes-2026-90
Preprint. Discussion started: 17 June 2026

eawe european academy of wind energy
Open Access WIND ENERGY SCIENCE DISCUSSIONS

A2 Planet bearing dimensions

The selection of planet bearings is based on catalog data from SKF, RKB, KOYO, and TIMKEN. To maximize the efficient use of available space, the bearing outer diameter $d_{\mathrm{o,PB}}$ is set equal to the planet gear inner diameter $d_{\mathrm{i,PB}}$, and the bearing face width b_{PB} is chosen as half of the gear width b:

$$d_{\mathrm{o,PB}} = d_{\mathrm{i},2}, \quad b_{\mathrm{PB}} = \frac{b}{2}. \tag{A23}$$

The remaining bearing specifications, including the bearing inner diameter, dynamic load rating, axial and radial load factors, and weight, are estimated using a second-degree polynomial curve fit based on catalog data (Tab. A2). This analytical approach is employed instead of a direct catalog lookup because it is computationally less demanding. Additionally, the limited availability of data for large-scale catalog bearings ($D > 1000\,\mathrm{mm}$), which are required for 15 MW drivetrains, would result in suboptimal designs.

A3 Component load calculation

The local component loads are calculated from rotor load time series simulated for each DLC with the aeroelastic model. In this step of the design process any drivetrain dynamics are neglected and the component loads are derived from static equilibrium equations.

(3) Gear loads

Only torque loads are considered for the gearbox design, as the four-point main shaft suspension and elastic gearbox coupling are designed to divert all non-torque loads into the bedplate.

The tangential gear forces in the sun–planet and ring–planet mesh for each stage k are then calculated using the number of planets $N_{\mathrm{P},k}$, pitch diameters $d_{\mathrm{p},1,k}$, $d_{\mathrm{p},3,k}$, and gear stage ratios $i_{\mathrm{st},k}$:

$$F_{\mathrm{t},12,k} = \frac{2T_{\mathrm{DEL}}}{N_{\mathrm{P},k} \cdot d_{\mathrm{p},1,k} \cdot \prod_{i=1}^{k} i_{\mathrm{st},i}}, \tag{A24}$$

$$F_{\mathrm{t},23,k} = \frac{2T_{\mathrm{DEL}} \cdot (i_{\mathrm{st},k} - 1)}{N_{\mathrm{P},k} \cdot d_{\mathrm{p},3,k} \cdot \prod_{i=1}^{k} i_{\mathrm{st},i}}. \tag{A25}$$

(4) Planet bearing loads

The radial and axial planet bearing loads are computed under the assumption of equal load sharing among planets and between front and rear bearings:

$$F_{\mathrm{rad},k} = \frac{F_{\mathrm{t},12,k} + F_{\mathrm{t},23,k}}{2}, \tag{A26}$$

$$F_{\mathrm{ax},k} = F_{\mathrm{rad},k} \tan(\beta). \tag{A27}$$

(5) Stress cycle counting

For design against ULS (static safety), the extreme loads across all DLCs is selected

$$F_{\mathrm{ULS}} = \max_{i \in \mathrm{DLCs}} F_i \tag{A28}$$

https://doi.org/10.5194/wes-2026-90
Preprint. Discussion started: 17 June 2026

eawe european academy of wind energy
Open Access WIND ENERGY SCIENCE DISCUSSIONS

For design against FLS (dynamic safety) only DLC 1.2, normal turbine operation, is considered, which has the predominant effect on fatigue damage. The load duration distribution (LDD) method is employed to generate load cycle histograms from the torque time series, where $n_{i,j}$ are the cycle counts and $T_{i,j}$ are the load amplitudes. The histograms are summed over all bins i and environmental conditions j using the wind speed distribution p_j and the S–N curve exponent m to calculate the damage equivalent load F_{FLS}:

$$F_{\mathrm{FLS}} = \left(\sum_{j=1}^{N_{\mathrm{EC}}} p_j \cdot \sum_{i=1}^{N_{\mathrm{bins}}} \frac{n_{i,j}}{N_{\mathrm{eq}}} \cdot F_{i,j}^{m} \right)^{1/m} \tag{A29}$$

A4 Objective function calculation

The design objective is formulated as a multi-objective optimization problem, balancing drivetrain mass and efficiency. This is achieved using a weighting parameter $w \in [0,1]$, where $w = 1$ corresponds to pure mass minimization and $w = 0$ corresponds to pure efficiency maximization. The objective function is expressed as:

$$J = w \cdot \frac{W_{\mathrm{DT}}}{W_{\mathrm{ref}}} + (1-w) \cdot \frac{\eta_{\mathrm{ref}} - \eta_{\mathrm{DT}}}{\eta_{\mathrm{ref}}} \tag{A30}$$

where W_{DT} is the total drivetrain mass, η_{DT} is the drivetrain efficiency, W_{ref} and η_{ref} are normalization references taken from the lightest and most efficient designs in the Pareto front.

The total drivetrain weight is calculated as the sum of the gear stages $W_{\mathrm{St,k}}$, with a modification factor of $K_{\mathrm{GBH}} = 1.33$ to account for the gearbox housing, based on empirical data indicating that the housing amounts to 25–35% of the gearbox mass:

$$W_{\mathrm{DT}} = K_{\mathrm{GBH}} \sum_{k=1}^{3} W_{\mathrm{st,k}} \tag{A31}$$

The gear stage weight comprise the sun, planet and ring gears, the sun and planet shafts, the planet carrier and the planet bearing:

$$W_{\mathrm{St}} = W_{\mathrm{SG}} + W_{\mathrm{SS}} + N_{\mathrm{P}} \left(W_{\mathrm{PG}} + 2W_{\mathrm{PB}} + W_{\mathrm{PS}} \right) + W_{\mathrm{RG}} + W_{\mathrm{PLC}} \tag{A32}$$

where:

$$W_{\mathrm{SG}} = \rho \frac{\pi}{4} \left(d_{\mathrm{p,1}}^2 - d_{\mathrm{i,1}}^2 \right) b \quad \text{(Sun gear)} \tag{A33}$$

$$W_{\mathrm{PG}} = \rho \frac{\pi}{4} \left(d_{\mathrm{p,2}}^2 - d_{\mathrm{i,2}}^2 \right) b \quad \text{(Planet gear)} \tag{A34}$$

$$W_{\mathrm{RG}} = \rho \frac{\pi}{4} \left(d_{\mathrm{o,3}}^2 - d_{\mathrm{p,3}}^2 \right) b \quad \text{(Ring gear)} \tag{A35}$$

$$W_{\mathrm{SS}} = \rho \frac{\pi}{4} d_{\mathrm{SS}}^2 \cdot 2b \quad \text{(Sun shaft)} \tag{A36}$$

$$W_{\mathrm{PS}} = \rho \frac{\pi}{4} d_{\mathrm{PS}}^2 b \quad \text{(Planet shaft)} \tag{A37}$$

$$W_{\mathrm{PLC}} = \rho \frac{\pi}{4} a^2 b \quad \text{(Planet carrier)} \tag{A38}$$

$$W_{\mathrm{PB}} = \mathrm{f}(d_{\mathrm{o,PB}}, b_{\mathrm{PB}}) \quad \text{(Planet Bearing)} \tag{A39}$$

https://doi.org/10.5194/wes-2026-90
Preprint. Discussion started: 17 June 2026

eawe european academy of wind energy
Open Access WIND ENERGY SCIENCE DISCUSSIONS

The weight of the planet bearings are estimated using a second-degree polynomial curve fit based on catalog data (Fig. **??**).

The drivetrain efficiency η_{DT} is evaluated using the Niemann–Winter method (Niemann and Winter, 1983), which estimates gear mesh losses based on empirical correlations for the coefficient of friction under elastohydrodynamic lubrication (EHL) conditions.

The mesh power loss is computed from the friction coefficient, normal load, and sliding velocity at each mesh. The total drivetrain efficiency is then given by

$$\eta_{\mathrm{DT}} = 1 - \frac{P_{\mathrm{loss}}}{P_{\mathrm{in}}}, \tag{A40}$$

where P_{loss} is the sum of all gear mesh losses and P_{in} is the mechanical input power.

A5 Constraint calculation

The design constraints, summarized in Tab. 3, arise from reliability requirements for gears, bearings and shafts according to ISO 6336, ISO 281 and DIN 743, and from geometrical constrains to ensure correct tooth meshing. For each design iteration it is checked if the constraints are fulfilled.

(1) Flank safety

The safety against surface pitting (flank safety) S_{H} must exceed a minimum value of $S_{\mathrm{H,min}} = 1.25$ for all gear pairs according to ISO 6336-2. The flank safety is the ratio of the permissible contact stress σ_{HG} and the actual contact stress σ_{H}:

$$S_{\mathrm{H}} = \frac{\sigma_{\mathrm{HG}}}{\sigma_{\mathrm{H}}} > S_{\mathrm{H,min}} \tag{A41}$$

The permissible and actual contact stress are calculated as follows:

$$\sigma_{\mathrm{HG}} = \sigma_{\mathrm{Hlim}} Z_{\mathrm{NT}} Z_{\mathrm{L}} Z_{\mathrm{V}} Z_{\mathrm{R}} Z_{\mathrm{W}} Z_{\mathrm{X}}, \tag{A42}$$

$$\sigma_{\mathrm{H}} = \sigma_{\mathrm{H0}} Z_{\mathrm{B/D}} \sqrt{K_{\mathrm{A}} K_{\gamma} K_{\mathrm{V}} K_{\mathrm{H}\beta} K_{\mathrm{H}\alpha}}, \tag{A43}$$

$$\sigma_{\mathrm{H0}} = Z_{\mathrm{H}} Z_{\mathrm{E}} Z_{\varepsilon} Z_{\beta} \sqrt{\frac{F_{\mathrm{t}}}{d_1 b} \frac{u+1}{u}}, \tag{A44}$$

with the Z- and K-factors according to Tab. A1, the gear force F_t, the pitch diameter d_1, the gear facewidth b and the tooth ratio u.

(2) Root safety

The minimum safety against tooth root cracks of $S_{\mathrm{F,min}} = 1.56$ must be satisfied according to ISO 6336-3. The root safety is the ratios of the permissible bending stress σ_{FG} and the actual bending stress σ_{F}:

$$S_{\mathrm{F}} = \frac{\sigma_{\mathrm{FG}}}{\sigma_{\mathrm{F}}} > S_{\mathrm{F,min}}. \tag{A45}$$

https://doi.org/10.5194/wes-2026-90
Preprint. Discussion started: 17 June 2026

The permissible and actual bending stress are given by:

$$\sigma_{\mathrm{FG}} = \sigma_{\mathrm{Flim}} Y_{\mathrm{ST}} Y_{\mathrm{NT}} Y_{\delta\mathrm{relT}} Y_{\mathrm{RrelT}} Y_{\mathrm{X}} Y_{\mathrm{M}}, \tag{A46}$$

$$\sigma_{\mathrm{F}} = \sigma_{\mathrm{F0}} K_{\mathrm{A}} K_{\gamma} K_{\mathrm{V}} K_{\mathrm{F}\beta} K_{\mathrm{F}\alpha}, \tag{A47}$$

$$\sigma_{\mathrm{F0}} = Y_{\mathrm{F}} Y_{\mathrm{S}} Y_{\beta} Y_{\mathrm{B}} Y_{\mathrm{DT}} \frac{F_{\mathrm{t}}}{b m_{\mathrm{n}}}, \tag{A48}$$

where the Y- and K-factors are listed in Tab. A1.

(6) Transmission ratio condition

The transmission ratio condition ensures that the actual gear stage ratios $\hat{i}_{\mathrm{st}}$ given by the sun and ring gear tooth numbers agree with the target gear ratio i_{st} within a tolerance of 2%:

$$\frac{\hat{i}_{\mathrm{st}} - i_{\mathrm{st}}}{i_{\mathrm{st}}} < \Delta i_{\mathrm{st}} \tag{A49}$$

$$\hat{i}_{\mathrm{st}} = 1 + \frac{z_3}{z_1} \tag{A50}$$

(7) Adjacency condition

The adjacency condition is in place to avoid tooth interference of neighboring planet gears and is given by:

$$d_{\mathrm{a},2} < 2a \sin\left(\frac{\pi}{N_{\mathrm{p}}}\right) \tag{A51}$$

(8) Assembly condition

The assembly condition is necessary to ensure that the planets can be physically assembled correctly. It states that the sum of the ring and sun gear tooth numbers must be a multiple of the number of planets:

$$\mathrm{mod}\,(z_3 + z_1, N_{\mathrm{p}}) = 0 \tag{A52}$$

(3) Bearing safety

The planet and main bearings must fulfill a minimum nominal lifetime of 25 years according to ISO 281:

$$L_{10h} > L_{10h,min}. \tag{A53}$$

The bearing nominal lifetime is calculated with the radial and axial loads $F_{\mathrm{rad}}, F_{\mathrm{ax}}$, the bearing specific load factors X_1, Y_1, the dynamic load rating C_1 and the shaft speed n in rpm:

$$P = X_1 \cdot F_{\mathrm{rad}} + Y_1 \cdot F_{\mathrm{ax}} \tag{A54}$$

$$L_{10} = \left(\frac{C_1}{P}\right)^{\frac{10}{3}} \tag{A55}$$

$$L_{10\mathrm{h}} = \frac{L_{10} \cdot 10^6}{n \cdot 60} \tag{A56}$$

https://doi.org/10.5194/wes-2026-90
Preprint. Discussion started: 17 June 2026

eawe european academy of wind energy
Open Access WIND ENERGY SCIENCE DISCUSSIONS

(4) ULS shaft safety

The gearbox shafts are designed against ULS and must meet a minimum shaft safety of $S_{\mathrm{ULS,min}} = 1.1$ according to DIN 743. The shaft ULS safety S_{ULS} is calculated as the ratio of the yield strength σ_{Y} and the van Mises stress σ_{Y}

$$S_{\mathrm{ULS}} = \frac{\sigma_{\mathrm{Y}}}{\sigma_{\mathrm{v,max}}} > S_{\mathrm{ULS,min}} \tag{A57}$$

The gearbox shafts are predominantly loaded by torque and have a cylindrical shape. Therefore the van Mises stress is only a function of the respective sun and planet shaft torque T_{ULS} and diameters d

$$\sigma_{\mathrm{v,max}} = \sqrt{3}\frac{16 T_{\mathrm{ULS}}}{\pi d^3} \tag{A58}$$

The main shaft is loaded by torque, pitch and yaw bending moments and has a tapered geometry with varying outer and inner diameters $D(x), d(x)$. The thrust is assumed to have a small impact on maximum stresses. In this case, the van Mises stress is calculated as follows.

$$I_{\mathrm{y}}(x) = I_{\mathrm{z}}(x) = 2J(x) = \frac{\pi}{64}\left(D(x)^4 - d(x)^4\right), \tag{A59}$$

$$\sigma_{\mathrm{y}}(x) = \frac{M_{\mathrm{MS,y}}(x) \cdot D(x)}{2I_{\mathrm{y}}(x)}, \tag{A60}$$

$$\sigma_{\mathrm{z}}(x) = \frac{M_{\mathrm{MS,z}}(x) \cdot D(x)}{2I_{\mathrm{z}}(x)}, \tag{A61}$$

$$\tau(x) = \frac{M_{\mathrm{MS,x}}(x) \cdot D(x)}{2J(x)}, \tag{A62}$$

$$\sigma_{\mathrm{v}}(x) = \sqrt{\sigma_{\mathrm{y}}^2 + \sigma_{\mathrm{z}}^2 + 3\tau^2}, \tag{A63}$$

$$\sigma_{\mathrm{v,max}} = \max(\sigma_{\mathrm{v}}(x)), \tag{A64}$$

https://doi.org/10.5194/wes-2026-90
Preprint. Discussion started: 17 June 2026

eawe european academy of wind energy
Open Access WIND ENERGY SCIENCE DISCUSSIONS

References

ISO 6336-2: Calculation of Load Capacity of Spur and Helical Gears – Calculation of Surface Durability (Pitting), 2006.

ISO 281: Rolling Bearings – Dynamic Load Ratings and Rating Life, 2007.

DIN 743: Calculation of Load Capacity of Shafts and Axles, 2012.

Barter, G. E. et al.: Beyond 15 MW: A cost of energy perspective on the next generation of drivetrain technologies for offshore wind turbines, Applied Energy, 344, 121 272, 2023.

Chong, T. H., Bae, I., and Park, G.-J.: A new and generalized methodology to design multi-stage gear drives by integrating the dimensional and the configuration design process, Mechanism and Machine Theory, 37, 295–310, https://doi.org/10.1016/S0094-114X(01)00078-7, 2002.

Driot, N. and Perret-Liaudet, J.: Variability of modal behavior in terms of critical speeds of a gear pair due to manufacturing errors and shaft misalignments, Journal of Sound and Vibration, 292, 824–843, https://doi.org/10.1016/j.jsv.2005.09.031, 2006.

Forschungsvereinigung Antriebstechnik e.V. (FVA): FVA-Workbench, https://www.fva-service.de/en/fva-workbench, simulation and calculation platform for transmission systems, 2024.

Gaertner, E., Rinker, J., Sethuraman, L., Zahle, F., Anderson, B., Barter, G., Abbas, N., Meng, F., Bortolotti, P., Skrzypinski, W., et al.: Definition of the IEA 15-Megawatt Offshore Reference Wind Turbine, Technical Report NREL/TP-5000-75698, National Renewable Energy Laboratory (NREL), https://www.nrel.gov/docs/fy20osti/75698.pdf, 2020.

Garambois, P., Perret-Liaudet, J., and Rigaud, E.: NVH robust optimization of gear macro and microgeometries using an efficient tooth contact model, Mechanism and Machine Theory, 117, 78–95, https://doi.org/10.1016/j.mechmachtheory.2017.07.008, 2017.

Gupta, V. and Nejad, A. R.: Gradient-based System Optimization of Wind Turbine Main Bearing Assembly: Enhancing State-of-the-Art Open-Source MDAO Tools, manuscript in preparation, 2026.

Huynh, D. H. and Nguyen, L. H.: Optimization of Transmission Ratios in a Three-Stage Spur-Helical Gearbox Using an Analytical Sizing Algorithm and Differential Evolution, Results in Engineering, 28, 108 080, https://doi.org/10.1016/j.rineng.2025.108080, 2025.

Karmi, B., Saouab, A., Guerine, A., Bouaziz, S., Hami, A. E., Haddar, M., and Dammak, K.: Reliability based design optimization of a two-stage wind turbine gearbox, Mechanics & Industry, 25, 16, https://doi.org/10.1051/meca/2024010, 2024.

KISSsoft AG: KISSsoft — Systematic Calculation of Machine Elements, https://www.kisssoft.com, gearbox and machine element design software, 2022a.

KISSsoft AG: Efficient Layout Process of Cylindrical Gears with Manufacturing Constraints, https://www.kisssoft.com/en/products/publications/brochures/efficient-layout-process-of-cylindrical-gears-with-manufacturing-constraints, accessed: April 23, 2025, 2022b.

National Renewable Energy Laboratory (NREL): WISDEM: Wind-Plant Integrated System Design & Engineering Model, https://github.com/WISDEM/WISDEM, accessed: 2025-05-01, 2024.

Nejad, A. R. and et al.: Wind turbine drivetrains: state-of-the-art technologies and future development trends, Wind Energy Science, 7, 387–411, https://doi.org/10.5194/wes-7-387-2022, 2022.

Niemann, G. and Winter, H.: Maschinenelemente Band III: Getriebe allgemein, Zahnradgetriebe – Grundlagen, Stirnradgetriebe, Springer-Verlag, Berlin, Heidelberg, 2 edn., ISBN 978-3-540-12269-1, in German, 1983.

Patil, M., Ramkumar, P., and Shankar, K.: Multi-objective optimization of the two-stage helical gearbox with tribological constraints, Mechanism and Machine Theory, 138, 38–57, https://doi.org/10.1016/j.mechmachtheory.2019.03.037, 2019.

https://doi.org/10.5194/wes-2026-90
Preprint. Discussion started: 17 June 2026

Qin, Z., Wu, Y.-T., and Lyu, S.-K.: A Review of Recent Advances in Design Optimization of Gearbox, International Journal of Precision Engineering and Manufacturing, 19, 1753–1762, https://doi.org/10.1007/s12541-018-0203-z, 2018.

Rezaei, A., Ruiz Maestre, R., Touzon, I., Fernández Bejarano, J. L., and Panjwani, B.: D2.1 – Use Case Scenario Definition of the 15 MW Wind Turbine, Project Deliverable D2.1, Norwegian University of Science and Technology (NTNU), MADE4WIND Project, Horizon Europe, https://made4wind.eu/wp-content/uploads/2025/10/D2.1-Use-Case-Scenario-Definition.pdf, deliverable responsible: NTNU, 2024.

Romax Technology Ltd.: Romax Spectrum, https://www.romaxtech.com/software/romax-spectrum/, transmission and drivetrain design and analysis software, 2024.

Stefanović-Marinović, J., Perić, M., Miltenović, A., Marinković, D., and Cojbašić, : An Approach to Multicriteria Optimization of the Three-Stage Planetary Gear Train, Machines, 13, 978, https://doi.org/10.3390/machines13110978, 2025.

Zeller, T., Kühnert, M., Schmitt, M., Cujic, P., Bank, D., and Doppelbauer, M.: Toolbox for an Analytical Determination of a Gearbox-Generator-Combination, in: 2024 IEEE International Conference on Industrial Technology (ICIT), IEEE, Bristol, United Kingdom, https://doi.org/10.1109/ICIT58233.2024.10540802, 2024.